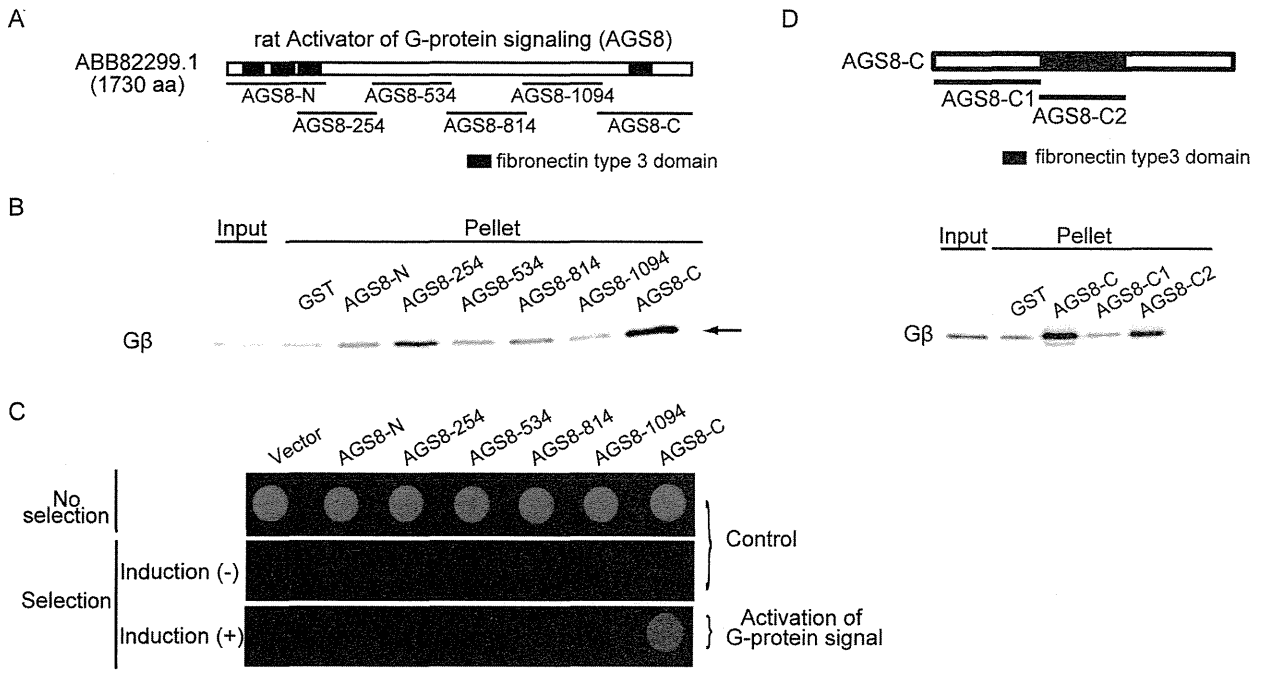

Figure 1. Determination of Gβγ interacting domain of the AGS8. (A) Schematic diagram of rat AGS8 and the AGS8 domains synthesized as GST-fusion proteins. Each GST protein fused with the following segment of rat AGS8 (ABB82299) respectively. AGS8-N: M^{1}- P^{370}, AGS8-254: A^{254}– R^{553}, AGS8-534: S^{534}– S^{833}, AGS8-814: S^{814}– R^{1113}, AGS8-1094: H^{1094}– D^{3280}, AGS8-C: A^{1359}– W^{1730}. (B) GST-pulldown assay of AGS8 domains with $G\beta_1\gamma_2$. AGS8 domains synthesized as GST-fusion proteins (300 nM) were incubated with recombinant human $G\beta_1\gamma_2$ (30 nM) in a total volume of 300 μl at 4°C. Proteins were then adsorbed to a glutathione matrix and retained G-protein subunits identified by immunoblotting following gel electrophoresis. The representative of 5 independent experiments with similar results. (C) Bioactivity of AGS8 domains on G-protein activation in cell. The yeast strain expressing human Gαs was transformed with AGS8 domains described in (A) into the pYES2-containing GAL1 promoter. The yeast strain was modified to grow without histidine on activation of G-protein. Induction(+): induction of translation of AGS8 domains by galactose. The representative of 4 independent experiments with similar results. (D) GST-pull down assay of AGS8-C segments with recombinant Gβγ. (*upper panel*) Schematic diagram of AGS8-C and the segments synthesized as GST-fusion proteins. Each GST protein fused with the following segment of rat AGS8 (ABB82299) respectively. AGS8-C1: A^{1359}– H^{1493}, AGS8-C2: A^{1494}– T^{1585}. (*lower panel*) GST-pulldown assay of AGS8 segments with $G\beta_1\gamma_2$. AGS8 domains synthesized as GST-fusion proteins (300 nM) were incubated with recombinant human $G\beta_1\gamma_2$ (30 nM) in a total volume of 300 μl at 4°C. Proteins were then adsorbed to a glutathione matrix and retained G-protein subunits identified by immunoblotting following gel electrophoresis. The representative of 4 independent experiments with similar results.
doi:10.1371/journal.pone.0091980.g001

protein CX43 under hypoxia, which results in decreased membrane permeability in the cardiomyocytes [13]. The change in localization and permeability of CX43 in the membrane is associated with hypoxia-induced apoptosis of the cardiomyocytes [14–16]. Therefore, we transferred the AGS8-peptide to cardiomyocytes and examined its effect on the internalization of CX43 induced by repetitive hypoxia (Fig. 4*A*).

The peptide was delivered to the cardiomyocytes by chemical reagent as described in "experimental procedures". Treatment of the cells with the chemical reagent and FITC-conjugated AGS8-peptide showed that the peptide was successfully delivered into the cardiomyocytes (Fig. 4*B*). The effect of the AGS8-peptide on internalization of CX43 was determined in the cardiomyocytes after hypoxic stress. CX43 was observed on the surface of the cardiomyocytes under normoxia (Fig. 4*B*), and its presence was decreased after exposure of the cardiomyocytes to repetitive hypoxia in the untransfected control cells and the cells exposed to transfection reagent alone (Fig. 4*B, 4C*). However, the AGS8-peptide dramatically blocked the internalization and degradation of CX43 induced by repetitive hypoxia (Fig. 4*B, 4C*). When the effect of FITC-conjugated AGS8-peptide was examined, FITC was observed in the cardiomyocytes under normoxia as well as hypoxia, and the hypoxia-induced internalization of CX43 was inhibited in FITC-positive cells (Fig. 4*B*).

The AGS8-peptide Inhibited the Decrease in Permeability of Connexin 43 Under Hypoxia

Loss of CX43 from the cell surface decreases influx and efflux of small molecules passing through CX43, and this effect is associated with apoptosis of the cardiomyocytes under hypoxia [13–16]. We next examined the ability of AGS8-peptide to block the change in permeability of CX43 by analyzing by the flux of the fluorescent dye, Lucifer Yellow (LY), which passes through CX43 as previously demonstrated [13]. LY in the culture medium was incorporated into cardiomyocytes under normoxia. The flux of dye was decreased after exposure of the cells to repetitive hypoxia in the control group as well as in the group exposed to transfection reagent alone (31.1±4.4%, 26.9±13.0%, respectively) (Fig. 5). However, the AGS8-peptide blocked the hypoxia-induced decrease in permeability in a dose-dependent manner. This observation is consistent with the immunofluorescence studies, in which CX43 was observed to remain at the cell surface after repetitive hypoxia in the presence of AGS8-peptide (Fig. 4).

The AGS8-peptide Protected Cardiomyocytes from Hypoxia-induced Apoptosis

To examine the effect of AGS8 peptide on apoptosis of the cardiomyocytes, cultured cardiomyocytes were sequentially ex-

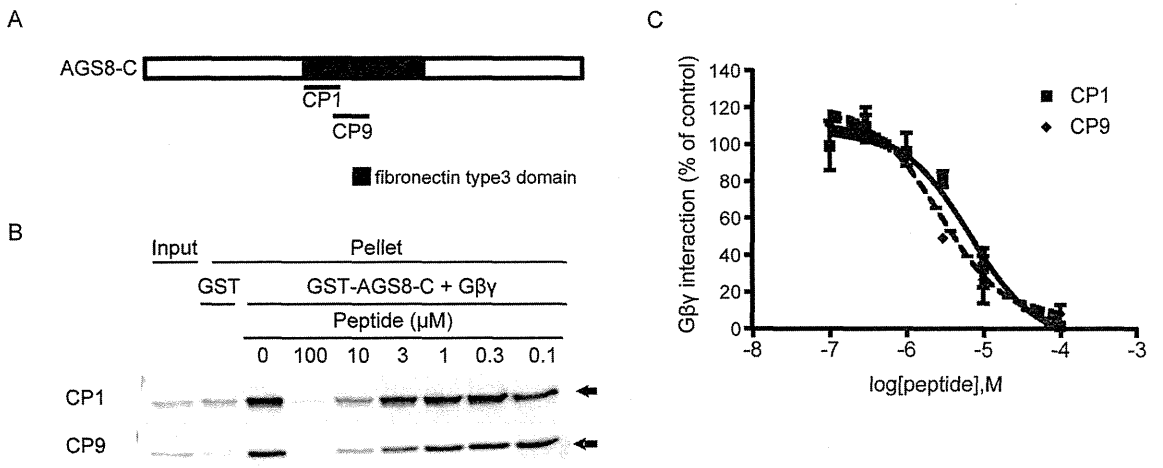

Figure 2. Development of AGS8 peptide. (A) Schematic diagram of AGS8-C and the AGS8-peptides (CP1 and CP9) which inhibited AGS8-Gβγ interaction. The AGS8-peptides were developed based on amino acid sequences of the Gβγ interaction domain of AGS8. CP1 and CP2 represented A^{1494}– V^{1522} and S^{1508}– I^{1537} of rat AGS8 (ABB82299) respectively. (B) The example of GST-pulldown assay of GST-AGS8-C with $G\beta_1\gamma_2$. GST-fusion protein (100 nM) was incubated with recombinant human $G\beta_1\gamma_2$ (10 nM) in the presence of AGS8-peptides (CP1 or CP9). Proteins were then adsorbed to a glutathione matrix and retained G-protein subunits identified by immunoblotting following gel electrophoresis. The representative of 6 independent experiments with similar results. (C) The densitometric analysis of GST-pulldown assay of GST-AGS8-C with $G\beta_1\gamma_2$ in the presence of AGS8-peptides. n = 6 with peptides of ~97% HPLC purity.
doi:10.1371/journal.pone.0091980.g002

posed to 1% oxygen for 6 h, then to 12 h of normoxia to induce hypoxia-mediated cell death (Fig. 6*A*) [13]. Hypoxia/reoxygenation markedly increased the number of apoptotic cardiomyocytes, as determined by TUNEL or immunostaining of cleaved caspase-3, in the untransfected control cells and those exposed to transfection reagent alone (Fig. 6B and 6C). However, AGS8-peptide successfully inhibited hypoxia-induced apoptosis, indicating a protective effect in cardiomyocytes. Additionally, the data indicated that, under normoxia, the AGS8-peptide did not influence apoptosis or the permeability of CX43 (Fig. 6*B and 6C*).

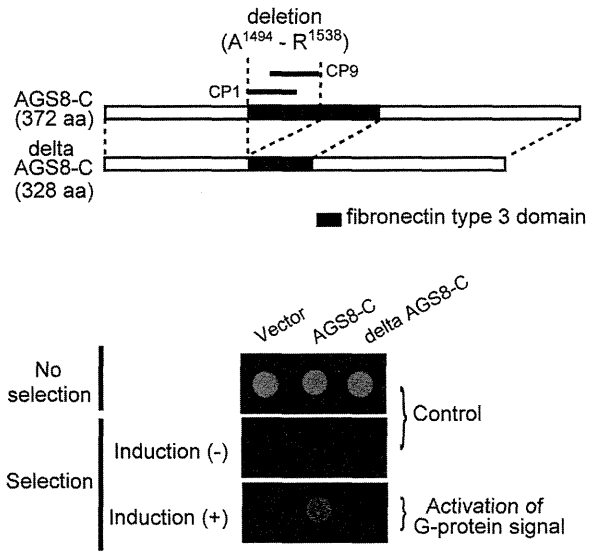

Figure 3. Effect of deletion of 45 amino acids of fibronectin type 3 domain. (A) Schematic diagram of C-terminal of AGS8 (AGS8-C) and the deleted mutant of AGS8-C (delta AGS8-C) lacking the first 45 amino acids of fibronectin type 3 domain, that are A^{1494} to R^{1538} of rat AGS8 (ABB82299). (B) Bioactivity of AGS8C and delta AGS8C on G-protein activation. The yeast strain expressing human Gαs was transformed with AGS8-C and delta AGS8-C in the pYES2-containing GAL1 promoter. The yeast strain was modified to grow without histidine on activation of G-protein. Induction (+): induction of translation of AGS8 domains by galactose. The representative of 4 independent experiments with similar results.
doi:10.1371/journal.pone.0091980.g003

Advantage of the AGS8-peptide for Targeted Disruption of the Gβγ Pathway

The data presented thus far indicated that the AGS8-peptide blocked the AGS8-Gβγ interaction and the signaling events the downstream of AGS8-Gβγ. We next asked whether inhibition of the Gβγ-mediated signal generally had a cardioprotective effect as was observed with the AGS8-peptide. Gallein is an inhibitor of Gβγ-mediated signaling that occupies a "common" interaction surface of Gβγ and inhibits the interaction of Gβγ-regulated proteins with Gβγ [25]. Thus, gallein is expected to block a wide range of Gβγ signals in cells, including CX43 regulation mediated by AGS-Gβγ. We previously demonstrated that gallein completely inhibits hypoxia-induced internalization of CX43 at 100 μM, as observed in the knockdown of AGS8, but not at 1 μM [13].

Here, we first examined the influence of the AGS8-peptide and gallein on the viability of cells. Cardiomyocytes were incubated with gallein for 24 h, and their viability was determined by MTT assay. Even the lowest concentration of gallein (1 μM) caused damage in the cardiomyocytes, indicating that broad inhibition of Gβγ did not have a protective effect (Fig. 7). In contrast, the AGS8-pepetide did not show cytotoxicity at 1 μM, the concentration that completely blocked the AGS8-Gβγ–mediated signal event. This suggests that the AGS8-peptide is a promising candidate for protection of cardiomyocytes from hypoxia-mediated apoptosis.

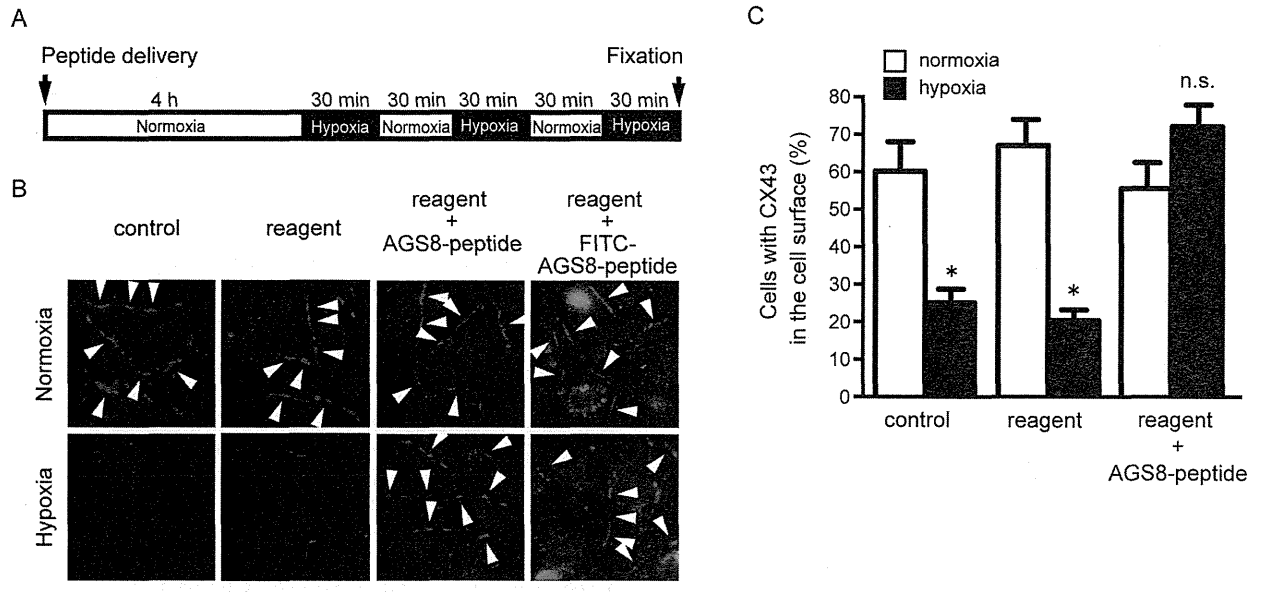

Figure 4. Effect of AGS8-peptide on localization of connexin 43 (CX43) of cultured cardiomyocytes. (A) Cardiomyocytes were exposed 3 times to 30 min of hypoxia (1% oxygen) intermittent with 30 min of reoxygenation 4 h after (without or with) transfection of AGS8-peptide (1 μM) or FITC-conjugated AGS8-peptide (1 μM). (B) Localization of CX43 in the cardiomyocytes under normoxia and hypoxia. The figures demonstrated in the triple color of CX43 (*red, arrow*), nuclei (DAPI, *blue*) and FITC-conjugated AGS8-peptide (*green*). The representative of 5 independent experiments with similar results. (C) The number of cardiomyocytes expressing CX43 in the cell surface were counted. Please note that ~ 90% cells were detectable at the point of fixation. Data are represent 170–260 cells from 5 of independent experiments. *, $p<0.05$ vs normoxia group.
doi:10.1371/journal.pone.0091980.g004

Discussion

AGS8-peptide, the sequence of which was derived from the amino-acid sequences of the Gβγ-binding domain of AGS8, blocked the association of AGS8 with Gβγ and inhibited AGS8-mediated events under hypoxia. Notably, AGS8-peptide inhibited the change in permeability of cell-surface CX43 and the apoptosis of cardiomyocytes. AGS8-peptide did not show cytotoxicity under normoxia, in contrast to the small molecule gallein, which produced deleterious effects by general inhibition of Gβγ-signaling. These data indicate that the AGS8-Gβγ complex plays a pivotal role in triggering the hypoxia-induced apoptosis of cardiomyocytes. Furthermore, they suggest an advantage of targeted disruption of G-protein signaling by the AGS-based peptide in protecting cardiomyocytes from hypoxia-induced apoptosis.

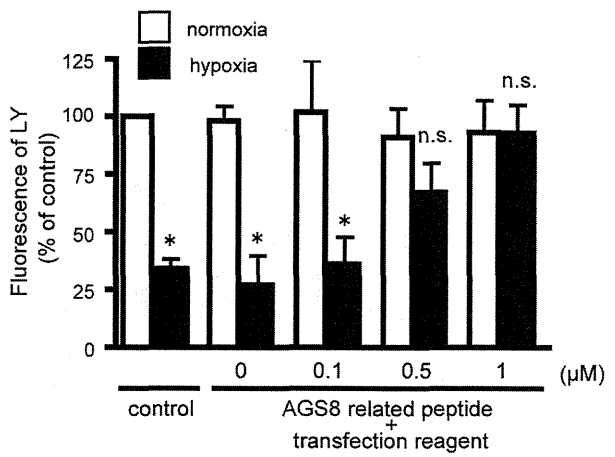

Figure 5. Uptake of connexin selective fluorescence dye, Lucifer Yellow (LY) to the cardiomyocytes. Cells were incubated with 1 mM of LY for 45 min in normal culture medium. Excess LY was removed and cells were rinsed with PBS. The fluorescence of LY was evaluated by inverted fluorescence microscope. The fluorescence of LY was quantified by the intensity of fluorescence of 10 randomly selected fields. The non-selective binding and/or incorporation of LY was determined fluorescence in the presence of a connexin hemichannel blocker, 50 μM of Lanthanum which was added 30 min prior to LY. *, $p<0.05$ vs cells in normoxia; *n.s.*, not statistically significant. N = 4 from 4 independent experiments.
doi:10.1371/journal.pone.0091980.g005

Several peptides have been developed to manipulate the broad signal initiated by accessory proteins for G-proteins. For example, an inhibitor of accessory proteins for heterotrimeric G-protein has been developed for RGS proteins. RGS proteins share 120–130 amino acids of an RGS-homology domain, which interact with the Gα subunit and accelerate GTPase activity [26,27]. RGS-peptides, which were designed on the basis of the X-ray structure of the Gαi switch I region of RGS4-Gαi, successfully modulate muscarinic receptor-regulated potassium currents in atrial myocytes [28]. RGS-peptides were initially designed to mimic the surface of G-protein to inhibit GAP activity, which produced the potential to suppress many events mediated by a variety of RGS proteins. As another example, a peptide, the sequence of which is based on G-protein regulatory (GPR) or GoLOCO motifs, is a cassette of 20–25 amino acids that stabilizes the GDP-bound conformation of Gα and clearly inhibits Gαi activation in vitro, suggesting its potential as an inhibitor of general Gαi signaling in cells [29].

Alternatively, the AGS8 peptide was designed on the basis of the AGS-Gβγ interface, with the objective of suppressing the specific signal evoked by AGS-Gβγ for all Gβγ signaling. It has been demonstrated that Gβγ-interacting proteins share an overlapping

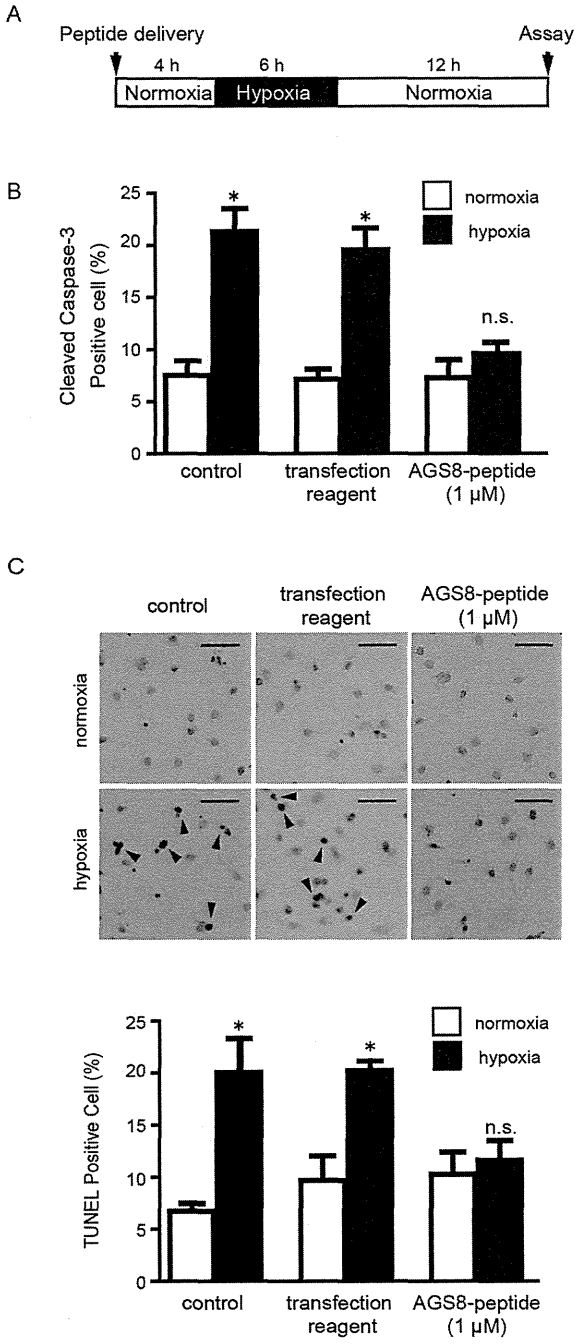

Figure 6. Effect of AGS8 peptide on hypoxia-induced apoptosis of cardiomyocytes. (A) Neonatal cardiomyocytes were exposed to hypoxia (1% oxygen) or normoxia as indicated duration without or with introduction of AGS8-peptide. Apoptosis was assessed by immunofluorescent detection of the active form of caspase-3 (cleaved caspase-3) (B) or TUNEL stain (C) as described in the experimental procedures. (C) Upper panel indicates representative apoptotic (*dark blue, arrow*) and non-apoptotic cells (*red*) after TUNEL staining. Scale bars indicate 100 μm. Approximately 3000 cells of 10 independent fields were counted for each experiments. A separate experiment indicated that AGS8-peptide did not influence the level of AGS8 within the 4-h treatment (1.0 μM peptide; 98.2±7.3% versus no reagent alone group, not statistically significant, $n=4$). *, $p<0.05$ vs cells in normoxia; *n.s.*, not statistically significant. N = 5 from 5 independent experiments.
doi:10.1371/journal.pone.0091980.g006

interface on the surface of Gβγ [30,31]. We previously demonstrated that the Gβγ-interacting surface of AGS8 includes the shared-site [32]. However, the entire Gβγ-interacting surface of AGS8 may include an additional interface, which is required to form an AGS8-specific signal complex. Our results indicated that 45 amino acids were required to evoke cell signaling by the AGS-Gβγ complex. The amino acid sequence of this domain did not have similarity to other known Gβγ interfaces [33–35], suggesting this sequence represents the AGS8-specifc interface that forms this particular complex. In fact, the AGS8-peptide designed to recognize this region successfully inhibited formation of the AGS8-Gβγ complex and subsequent cell events mediated by AGS8-Gβγ. However, currently, there is not enough information to determine whether the AGS8-peptide covers the common Gβγ interface or influences the interaction of Gβγ with other molecules. These issues are to be investigated elsewhere.

AGS-Gβγ–mediated signaling is required for hypoxia-induced apoptosis of cardiomyocytes [13]. Gβγ is known to conduct pro-apoptotic signaling via p38MAPK, JNK, or PLCβ, whereas anti-apoptotic signaling is also mediated by Gβγ via PI3K-Akt or ERK depending on type of cell and stimulus [36–39]. Although the involvement of these Gβγ-mediated pathways in the AGS-Gβγ pathway or other players in the AGS-Gβγ protein complex are yet to be determined, the current data indicate the presence of a critical signaling pathway mediated by the AGS8-Gβγ complex leading to apoptosis in cardiomyocytes.

The channel protein CX43 plays a role in the apoptotic process by regulating the permeability of small molecules, including adenosine 5′-triphosphate, adenosine diphosphate, adenosine, cAMP, inositol-1,4,5-triphosphate, glutamate, and glutathione [14,15,40–42]. In response to hypoxia, AGS8 organizes the complex that includes Gβγ, CX43, and possibly kinases that initiate phosphorylation of CX43 [13]. Multiple phosphorylation sites on CX43 are regulated by specific kinases under ischemic

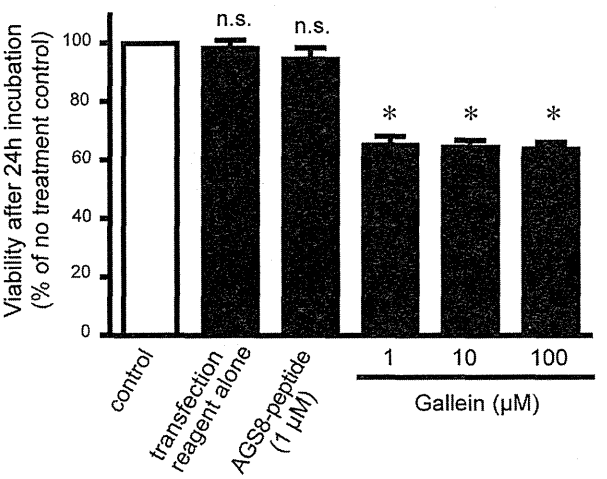

Figure 7. Effect of AGS8-peptide or Gallein on the viability of cardiomyocytes determined by MTT assay. Neonatal cardiomyocytes were cultured for 24 h with AGS8-peptide or Gallein. Gallein occupied a "common" interaction surface of Gβγ and inhibited its interaction with Gβγ-regulated proteins. *, $p<0.05$ vs cells in normoxia; *n.s.*, not statistically significant. N = 5 from 5 independent experiments.
doi:10.1371/journal.pone.0091980.g007

conditions, and each phosphorylation critically influences the permeability and localization of CX43 in the sarcolemma [43,44]. The inhibition of internalization of CX43 by AGS8-peptide may suggest that AGS8-peptide blocked the recruitment of components into the complex and/or phosphorylation of CX43 within the complex. AGS8 may play a role in separating the hypoxic/ischemic cardiomyocytes from healthy tissue by disconnecting the gap junction, which can contribute to arrhythmia and contraction failure during ischemia. Although the validity of this hypothesis is yet to be tested in confirmed or animal models, our observations support this possibility.

Myocardial ischemia activates multiple cascades that initiate intracellular ionic and chemical changes leading cell to death [17,18]. Although great efforts have been made over many years, therapeutic approaches to ischemic heart disease still need further development [45,46]. We previously demonstrated that AGS8-Gβγ signaling was activated under hypoxia and did not constitutively stimulate the apoptotic pathway, because the pro-apoptotic effects of AGS were not observed in cells cultured under normoxia [13]. In fact, AGS8-peptide effectively protected cardiomyocytes from hypoxia-mediated cell death, but did not cause cell damage under normoxia. Thus, AGS8-peptide has the potential to save a subpopulation of cardiomyocytes exposed to hypoxia without producing damage to the entire myocardium. This is an advantage of targeted disruption of specific signaling by AGS8-peptide, and it stands in contrast to the deleterious effects caused by general inhibition of Gβγ signaling with gallein.

Peptide-based reagents designed from the sequences of accessory proteins for heterotrimeric G-protein have potential to manipulate alternative signaling events distinct from GPCR-mediated G-protein signaling. At this stage, the potential of peptide-based reagents, including AGS8-peptide, remains limited by their ability to penetrate the membrane, their stability, and the modes of delivery available for their use as clinical drugs. The strategies for effective delivery of therapeutic peptides into the cell include conjugation with cell-penetrating peptides, incorporation into polymeric nanoparticles, and virus-mediated release of peptides [47–49]. Each strategy still has challenges with respect to the efficiency or selectivity of delivery as well as safety in healthy tissues or cells [47,49,50]. Although intracellular use of peptide targeting is not yet a common practice, delivery systems are continuously being developed, which will increase the potential for use of peptide-targeting therapy. We have demonstrated the possibility of regulating intracellular signaling mediated by accessory proteins for heterotrimeric G-protein, which could be a starting point for development of peptides or compounds to regulate AGS8-Gβγ signaling.

Targeted disruption of the interaction of G-protein with accessory proteins for heterotrimeric G-protein is a promising therapeutic strategy because these molecules mediate critical signaling distinct from the receptor-mediated pathway. In this study, we demonstrated that AGS8-peptide could be part of a novel therapeutic approach for the protection of ischemia in the heart that has enhanced specificity and fewer side effects. Although efforts to intervene in G-protein signaling have been focused on the interface of the GPCR-heterotrimeric G-protein, our data highlight the advantages of accessory proteins for heterotrimeric G-protein as alternative therapeutic targets in human diseases.

Acknowledgments

We acknowledge Dr. James R. Broach (Molecular Biology, Princeton University, NJ, USA) and Cadus Pharmaceutical Corp. (NY, USA) for providing yeast strains used in this study.

Author Contributions

Conceived and designed the experiments: M. Sato. Performed the experiments: M. Sato MH HS YY. Analyzed the data: M. Sakima AAM TF UY SO. Contributed reagents/materials/analysis tools: UY SO TF YI. Wrote the paper: M. Sato.

References

1. Birnbaumer L (2007) Expansion of signal transduction by G proteins. The second 15 years or so: from 3 to 16 alpha subunits plus betagamma dimers. Biochim Biophys Acta 1768: 772–793.
2. Sato M, Blumer JB, Simon V, Lanier SM (2006) ACCESSORY PROTEINS FOR G PROTEINS: Partners in Signaling. Annu Rev Pharmacol Toxicol 46: 151–187.
3. Blumer JB, Smrcka AV, Lanier SM (2007) Mechanistic pathways and biological roles for receptor-independent activators of G-protein signaling. Pharmacol Ther 113: 488–506.
4. Sjogren B (2011) Regulator of G protein signaling proteins as drug targets: current state and future possibilities. Adv Pharmacol 62: 315–347.
5. Sato M (2013) Roles of Accessory Proteins for Heterotrimeric G-Protein in the Development of Cardiovascular Diseases. Circ J.
6. Cismowski MJ, Ma C, Ribas C, Xie X, Spruyt M, et al. (2000) Activation of heterotrimeric G-protein signaling by a ras-related protein. Implications for signal integration. J Biol Chem 275: 23421–23424.
7. McGrath MF, Ogawa T, de Bold AJ (2012) Ras dexamethasone-induced protein 1 is a modulator of hormone secretion in the volume overloaded heart. Am J Physiol Heart Circ Physiol 302: H1826–1837.
8. Wieland T, Mittmann C (2003) Regulators of G-protein signalling: multifunctional proteins with impact on signalling in the cardiovascular system. Pharmacol Ther 97: 95–115.
9. Gu S, Cifelli C, Wang S, Heximer SP (2009) RGS proteins: identifying new GAPs in the understanding of blood pressure regulation and cardiovascular function. Clin Sci (Lond) 116: 391–399.
10. Zhang P, Mende U (2011) Regulators of G-protein signaling in the heart and their potential as therapeutic targets. Circ Res 109: 320–333.
11. Sato M, Hiraoka M, Suzuki H, Bai Y, Kurotani R, et al. (2011) Identification of transcription factor E3 (TFE3) as a receptor-independent activator of Galpha16: gene regulation by nuclear Galpha subunit and its activator. J Biol Chem 286: 17766–17776.
12. Sato M, Cismowski MJ, Toyota E, Smrcka AV, Lucchesi PA, et al. (2006) Identification of a receptor-independent activator of G protein signaling (AGS8) in ischemic heart and its interaction with Gbetagamma. Proc Natl Acad Sci U S A 103: 797–802.
13. Sato M, Jiao Q, Honda T, Kurotani R, Toyota E, et al. (2009) Activator of G protein signaling 8 (AGS8) is required for hypoxia-induced apoptosis of cardiomyocytes: role of G betagamma and connexin 43 (CX43). J Biol Chem 284: 31431–31440.
14. Harris AL (2007) Connexin channel permeability to cytoplasmic molecules. Prog Biophys Mol Biol 94: 120–143.
15. Rodriguez-Sinovas A, Cabestrero A, Lopez D, Torre I, Morente M, et al. (2007) The modulatory effects of connexin 43 on cell death/survival beyond cell coupling. Prog Biophys Mol Biol 94: 219–232.
16. Zhang SS, Shaw RM (2013) Multilayered regulation of cardiac ion channels. Biochim Biophys Acta 1833: 876–885.
17. Yellon DM, Hausenloy DJ (2007) Myocardial reperfusion injury. N Engl J Med 357: 1121–1135.
18. Bishopric NH, Andreka P, Slepak T, Webster KA (2001) Molecular mechanisms of apoptosis in the cardiac myocyte. Curr Opin Pharmacol 1: 141–150.
19. Sato M, Gettys TW, Lanier SM (2004) AGS3 and signal integration by Galpha(s)- and Galpha(i)-coupled receptors: AGS3 blocks the sensitization of adenylyl cyclase following prolonged stimulation of a Galpha(i)-coupled receptor by influencing processing of Galpha(i). J Biol Chem 279: 13375–13382.
20. Sato M, Ribas C, Hildebrandt JD, Lanier SM (1996) Characterization of a G-protein activator in the neuroblastoma-glioma cell hybrid NG108-15. J Biol Chem 271: 30052–30060.
21. Sato M, Ohsaki Y, Tobise K (1995) Transforming growth factor-beta 1 proliferated vascular smooth muscle cells from spontaneously hypertensive rats. Am J Hypertens 8: 160–166.
22. Thuc LC, Teshima Y, Takahashi N, Nagano-Torigoe Y, Ezaki K, et al. (2010) Mitochondrial K(ATP) channels-derived reactive oxygen species activate pro-survival pathway in pravastatin-induced cardioprotection. Apoptosis 15: 669–678.
23. Cismowski MJ, Takesono A, Ma C, Lizano JS, Xie X, et al. (1999) Genetic screens in yeast to identify mammalian nonreceptor modulators of G-protein signaling. Nat Biotechnol 17: 878–883.
24. Takesono A, Cismowski MJ, Ribas C, Bernard M, Chung P, et al. (1999) Receptor-independent activators of heterotrimeric G-protein signaling pathways. J Biol Chem 274: 33202–33205.

25. Lehmann DM, Seneviratne AM, Smrcka AV (2008) Small molecule disruption of G protein beta gamma subunit signaling inhibits neutrophil chemotaxis and inflammation. Mol Pharmacol 73: 410–418.
26. Sjogren B, Blazer LL, Neubig RR (2010) Regulators of G protein signaling proteins as targets for drug discovery. Prog Mol Biol Transl Sci 91: 81–119.
27. Kimple AJ, Bosch DE, Giguere PM, Siderovski DP (2011) Regulators of G-protein signaling and their Galpha substrates: promises and challenges in their use as drug discovery targets. Pharmacol Rev 63: 728–749.
28. Roof RA, Jin Y, Roman DL, Sunahara RK, Ishii M, et al. (2006) Mechanism of action and structural requirements of constrained peptide inhibitors of RGS proteins. Chem Biol Drug Des 67: 266–274.
29. Peterson YK, Bernard ML, Ma H, Hazard S 3rd, Graber SG, et al. (2000) Stabilization of the GDP-bound conformation of Gialpha by a peptide derived from the G-protein regulatory motif of AGS3. J Biol Chem 275: 33193–33196.
30. Ford CE, Skiba NP, Bae H, Daaka Y, Reuveny E, et al. (1998) Molecular basis for interactions of G protein betagamma subunits with effectors. Science 280: 1271–1274.
31. Smrcka AV (2008) G protein betagamma subunits: Central mediators of G protein-coupled receptor signaling. Cell Mol Life Sci 65: 2191–2214.
32. Yuan C, Sato M, Lanier SM, Smrcka AV (2007) Signaling by a non-dissociated complex of G Protein betagamma and alpha subunits stimulated by a receptor-independent activator of G protein signaling, AGS8. J Biol Chem 282: 19938–19947.
33. Touhara K, Inglese J, Pitcher JA, Shaw G, Lefkowitz RJ (1994) Binding of G protein beta gamma-subunits to pleckstrin homology domains. J Biol Chem 269: 10217–10220.
34. Chen J, DeVivo M, Dingus J, Harry A, Li J, et al. (1995) A region of adenylyl cyclase 2 critical for regulation by G protein beta gamma subunits. Science 268: 1166–1169.
35. Qin N, Platano D, Olcese R, Stefani E, Birnbaumer L (1997) Direct interaction of gbetagamma with a C-terminal gbetagamma-binding domain of the Ca2+ channel alpha1 subunit is responsible for channel inhibition by G protein-coupled receptors. Proc Natl Acad Sci U S A 94: 8866–8871.
36. New DC, Wu K, Kwok AW, Wong YH (2007) G protein-coupled receptor-induced Akt activity in cellular proliferation and apoptosis. FEBS J 274: 6025–6036.
37. Goldsmith ZG, Dhanasekaran DN (2007) G protein regulation of MAPK networks. Oncogene 26: 3122–3142.
38. Marinissen MJ, Gutkind JS (2001) G-protein-coupled receptors and signaling networks: emerging paradigms. Trends Pharmacol Sci 22: 368–376.
39. Adams JW, Brown JH (2001) G-proteins in growth and apoptosis: lessons from the heart. Oncogene 20: 1626–1634.
40. Shintani-Ishida K, Uemura K, Yoshida K (2007) Hemichannels in cardiomyocytes open transiently during ischemia and contribute to reperfusion injury following brief ischemia. Am J Physiol Heart Circ Physiol 293: H1714–1720.
41. Solan JL, Marquez-Rosado L, Sorgen PL, Thornton PJ, Gafken PR, et al. (2007) Phosphorylation at S365 is a gatekeeper event that changes the structure of Cx43 and prevents down-regulation by PKC. J Cell Biol 179: 1301–1309.
42. Bao X, Lee SC, Reuss L, Altenberg GA (2007) Change in permeant size selectivity by phosphorylation of connexin 43 gap-junctional hemichannels by PKC. Proc Natl Acad Sci U S A 104: 4919–4924.
43. Ek-Vitorin JF, King TJ, Heyman NS, Lampe PD, Burt JM (2006) Selectivity of connexin 43 channels is regulated through protein kinase C-dependent phosphorylation. Circ Res 98: 1498–1505.
44. Lampe PD, Cooper CD, King TJ, Burt JM (2006) Analysis of Connexin43 phosphorylated at S325, S328 and S330 in normoxic and ischemic heart. J Cell Sci 119: 3435–3442.
45. Windecker S, Bax JJ, Myat A, Stone GW, Marber MS (2013) Future treatment strategies in ST-segment elevation myocardial infarction. Lancet 382: 644–657.
46. Jneid H (2012) The 2012 ACCF/AHA Focused Update of the Unstable Angina/Non-ST-Elevation Myocardial Infarction (UA/NSTEMI) Guideline: a critical appraisal. Methodist Debakey Cardiovasc J 8: 26–30.
47. Clemons TD, Viola HM, House MJ, Iyer KS, Hool LC (2013) Examining efficacy of "TAT-less" delivery of a peptide against the L-type calcium channel in cardiac ischemia-reperfusion injury. ACS Nano 7: 2212–2220.
48. Flores-Munoz M, Godinho BM, Almalik A, Nicklin SA (2012) Adenoviral delivery of angiotensin-(1–7) or angiotensin-(1–9) inhibits cardiomyocyte hypertrophy via the mas or angiotensin type 2 receptor. PLoS One 7: e45564.
49. Svensen N, Walton JG, Bradley M (2012) Peptides for cell-selective drug delivery. Trends Pharmacol Sci 33: 186–192.
50. Jones AT, Sayers EJ (2012) Cell entry of cell penetrating peptides: tales of tails wagging dogs. J Control Release 161: 582–591.

Life Sciences 101 (2014) 43–48

Contents lists available at ScienceDirect

Life Sciences

journal homepage: www.elsevier.com/locate/lifescie

Geranylgeranylacetone protects the heart via caveolae and caveolin-3

Yasuo M. Tsutsumi [a,*], Rie Tsutsumi [b], Yousuke T. Horikawa [a], Yoko Sakai [a], Eisuke Hamaguchi [a], Yoshihiro Ishikawa [c], Utako Yokoyama [c], Asuka Kasai [a], Noriko Kambe [a], Katsuya Tanaka [a]

[a] Department of Anesthesiology, University of Tokushima, Tokushima, Japan
[b] Department of Nutrition, University of Tokushima, Tokushima, Japan
[c] Cardiovascular Research Institute, Yokohama City University, Yokohama, Japan

ARTICLE INFO

Article history:
Received 5 November 2013
Accepted 12 February 2014
Available online 26 February 2014

Keywords:
Geranylgeranylacetone
Caveolin
Caveolae
Cardiac protection
Heat shock protein

ABSTRACT

Aims: Geranylgeranylacetone (GGA) is commonly utilized to protect the gastric mucosa in peptic ulcer disease. Recently GGA has been shown to protect the myocardium from ischemia/reperfusion by activating heat shock proteins. However, the exact mechanism as to how GGA activates these protective proteins is unknown. Caveolae and caveolin-3 (Cav-3) have been implicated in ischemia, anesthetic, and opioid induced cardiac protection. Given the lipophilic nature of GGA it is our hypothesis that GGA induced cardiac protection requires caveolae and Cav-3.

Main methods: We used an in vivo mouse model of ischemia–reperfusion injury and performed biochemical assays in excised hearts.

Key findings: GGA treated control mice revealed increased caveolae formation and caveolin-3 in buoyant fractions, mediating heat shock protein 70 activation. Furthermore, control mice treated with GGA were protected against ischemia/reperfusion injury whereas Cav-3 knockout (Cav-3 KO) mice were not. Troponin levels confirmed myocardial damage. Finally, Cav-3 KO mice treated with GGA were not protected against mitochondrial swelling whereas control mice had significant protection.

Significance: This study showed that caveolae and caveolin-3 are essential in facilitating GGA induced cardiac protection by optimizing spatial and temporal signaling to the mitochondria.

Introduction

Geranylgeranylacetone (GGA), an acyclic polyisoprenoid, is commonly used as an oral anti-ulcer medication in Asia. This compound has been shown to be effective in protecting the gastric mucosa against insults without affecting gastric acid secretion (Fujimoto et al., 1982; Murakami et al., 1981). Oral GGA has been demonstrated to have protective effects on myocardial ischemia/reperfusion injury within the rat heart (Ooie et al., 2001). Yamanaka et al. suggested that GGA-induced cardiac preconditioning exerted protective effects on myocardial ischemia/reperfusion injury by mediating the activation of protein kinase C and heat shock protein (HSP) (Yamanaka et al., 2003). Further investigations demonstrated that GGA also prevented cellular endothelial damage (Zhu et al., 2005), diminished apoptosis and preserved mitochondrial respiratory function (Shinohara et al., 2007).

Structural scaffolding domains commonly organize signal transduction molecules and receptors. Caveolae are small membrane invaginations of the plasma membrane that are enriched in sphingolipids, cholesterol, and lipid rafts (Lisanti et al., 1994; Palade, 1953; Patel et al., 2008). Caveolins are the structural proteins of caveolae and are present in three isoforms, caveolin (Cav)-1, -2, and -3 (Lisanti et al., 1994; Patel et al., 2008). Additionally, many signaling molecules are known to localize in caveolae and interact with the scaffolding domain of caveolin. We have recently shown that both caveolae and Cav-3 were essential for ischemic (Horikawa et al., 2008; Tsutsumi et al., 2008), anesthetic (Horikawa et al., 2008), and opioid (Tsutsumi et al., 2010b) induced cardiac protection. It is our hypothesis that caveolin-3 and caveolae are also essential in GGA induced cardiac protection.

Materials and methods

Animals

All animals were treated in compliance with the Guidelines for Proper Conduct of Animal Experiment and Related Activities (Ministry of Education, Culture, Sports, Science and Technology of Japan) and the Guideline for Care and Use of Lab Animals at the University of

* Corresponding author at: Department of Anesthesiology, University of Tokushima, 3-18-15 Kuramoto, Tokushima 770-8503, Japan. Tel.: +81 88 633 7181; fax: +81 88 633 7182.
E-mail address: tsutsumi@tokushima-u.ac.jp (Y.M. Tsutsumi).

http://dx.doi.org/10.1016/j.lfs.2014.02.019
0024-3205/

Tokushima. Animal use protocols were approved by the Animal Care and Use Committee, the University of Tokushima. Male C57BL/6 mice (8–10 weeks old, 21–26 g body weight) were purchased from Japan SLC and Cav-3 knockout (Cav-3 KO) mice were created as reported previously (Hagiwara et al., 2000). Animals were randomly assigned into treatment groups by an independent observer. The animals were kept on a 12 hour light–dark cycle in a temperature-controlled room. GGA was provided by Eisai Co., Tokyo, Japan and was given by gavage at a dose of 200 mg/kg (dissolved with 0.4% lecithin in deionized water). Mice in the control group were given the same dose of vehicle.

Electron microscopy

Wild-type mice were given GGA or vehicle by oral gavage. Twenty four hours later, whole hearts were fixed with 2.5% glutaraldehyde in 0.1 M cacodylate buffer for 2 h at room temperature, post-fixed in 1% OsO_4 in 0.1 M cacodylate buffer (1 h), and uranyl acetate, dehydrated in a graded series of ethanol solutions, and embedded in epon epoxy resin. Sections were cut with a Reichert Ultracut E Ultramicrotome (Leica Microsystems, Wetzlar, Germany) and observed with an electron microscope (Hitachi H7650, Hitachi Co., Tokyo, Japan). Random sections were taken by an electron microscopy technician blinded to the treatments.

Sucrose density membrane fractionation

We performed whole left ventricle sucrose density membrane fractions as reported previously (Tsutsumi et al., 2008). Fraction samples 4–12 were used in immunoblot analyses. We defined fractions 4–6 as lipid rich–buoyant membrane fractions enriched in caveolae and proteins associated with caveolae. Fractions 9–12 were defined as non-buoyant fractions.

Immunoblot analysis

Proteins in whole left ventricle or membrane fractions were separated by SDS-PAGE 10% polyacrylamide precast gels (Bio-Rad Laboratories) and transferred to a polyvinylidene difluoride membrane by electroelution. Membranes were blocked in PBS containing 2.0% nonfat dry milk and incubated with primary antibody overnight at 4 °C. Bound primary antibodies were visualized using secondary antibodies conjugated with horseradish peroxidase from Santa Cruz Biotechnology (Santa Cruz) and ECL reagent from Amersham Pharmacia. All displayed bands migrated at the appropriate size, as determined by comparison to molecular weight standards (Santa Cruz Biotechnology).

Immunoprecipitation

Immunoprecipitation was performed using Protein A Sepharose CL-4B (GE Healthcare) as described previously (Hirose et al., 2011). Buoyant fraction samples were incubated with primary antibody for 3 h at 4 °C, immunoprecipitated overnight with protein-agarose at 4 °C, and then centrifuged for 5 min at 13,000 g. Protein-agarose pellets were washed 3 times. Wash buffer was removed and sample buffer was added, and then boiled for 5 min at 95 °C for immunoblotting.

Ischemia–reperfusion protocol and experimental groups

Cav-3 KO and control mice were randomly assigned to receive GGA or vehicle 24 h before ischemic injury. Mice were anesthetized with pentobarbital sodium (80 mg/kg i.p.) and mechanically ventilated by using a pressure-controlled ventilator (TOPO Ventilator, Kent Scientific) as described before (Tsutsumi et al., 2006, 2007). Core temperature was maintained with a heating pad and ECG leads were placed to record heart rate. The hemodynamic effects were measured through the right carotid artery cannulation with a 1.4F Mikro-tip pressure transducer (Model SPR-671, Millar Instruments), which was connected to an amplifier (Model TC-510, Millar Instruments) for determination of heart rate, arterial blood pressure, and rate pressure product.

Lethal ischemia was produced by occluding the left coronary artery with a 7–0 silk suture placed with a tapered BV-1 needle (Ethicon) for 30 min. After 30 min of occlusion, the ligature was released and the heart was reperfused for 2 h. After reperfusion, mice were heparinized, and the coronary artery was again occluded. The area at risk (AAR) was determined by staining with 1% Evans blue (1.0 mL, Sigma). The heart was immediately excised and cut into 1.0-mm slices (McIlwain tissue chopper; Brinkmann Instruments). Each slice of left ventricle (LV) was then counterstained with 2,3,5,-triphenyltetrazolium chloride (Sigma). After overnight storage in 10% formaldehyde, slices were weighed and visualized under a microscope (SZ61-TR, Olympus) equipped with a charge coupled device camera (DXM 1200F, Nikon). The images were analyzed (Image-Pro Plus, Media Cybernetics), and area at risk (AAR) and infarct size (IS) were determined by planimetry as previously described (Tsutsumi et al., 2008; Horikawa et al., 2008). Cardiac troponin I (cTnI) levels in the serum were measured using a High Sensitivity Mouse Cardiac Troponin-I ELISA Kit (Life Diagnostics) as described before (Tsutsumi et al., 2010a).

Mitochondrial isolation and swelling assay

Mice were anesthetized and hearts were harvested, immediately rinsed with PBS, and placed in homogenizer containing 4 mL sucrose buffer A (300 mM sucrose, 10 mM Tris–HCl, 2 mM EGTA and 5 mg/mL BSA, pH 7.4) on ice. Hearts were homogenized using 10 strokes and homogenate centrifuged at 2000 ×g for 2 min at 4 °C to remove cell debris. The supernatant was further centrifuged at 10,000 ×g for 30 min at 4 °C to sediment impure mitochondria. Mitochondrial pellet was purified and washed as described previously (Fridolfsson et al., 2012). 200 μL of mitochondria in sucrose buffer B (300 mM sucrose, 10 mM Tris–HCl, pH 7.4) was loaded on to 96-well plate and challenged with 100 μM $CaCl_2$ (2 mg/mL protein concentration). Absorbance was measured every 2 s for 600 measurements at 520 nm using a VarioSkan Flash spectrophotometer (Thermo Scientific). 250 nM cyclosporine A (Sigma) pretreatment of mitochondria was used to inhibit $CaCl_2$ induced mitochondrial swelling to confirm the mitochondrial permeability transition pore (mPTP) dependence of calcium-induced swelling.

Statistical analysis

Determination of all data was performed blinded to experimental groups for the observers. Data were analyzed using Prism 6.0 (GraphPad Software, Inc.). Statistical analyses for Western blot studies were performed using Student's *t*-tests. When one-way ANOVA was needed, the Bonferroni post-hoc test was used. All data are expressed as mean ± SD. Statistical significance was defined as $P < 0.05$

Results

The effect of GGA on cardiac membrane caveolae was assessed by pre-treating mice with and without GGA and performing electron microscopy analysis. Representative electron microscopy images show that pretreatment of GGA increased membrane caveolae compared to vehicle treated control animals (Fig. 1). However, Cav-3 KO mice had significantly decreased caveolae with no significant change after GGA treatment (data not shown). To verify these findings, hearts from GGA and vehicle control animals were fractionated on a discontinuous sucrose gradient and analyzed for protein content. GGA increased both Cav-3 protein expression and HSP 70 expression in buoyant fractions 4–6, which are associated with caveolae (Fig. 2A and 2B). Additionally, immunoprecipitation experiments showed that GGA treated mice resulted in HSP 70 associated with Cav-3 in buoyant fractions (Fig. 2C), suggesting that Cav-3 is essential for HSP 70 localization and activation.

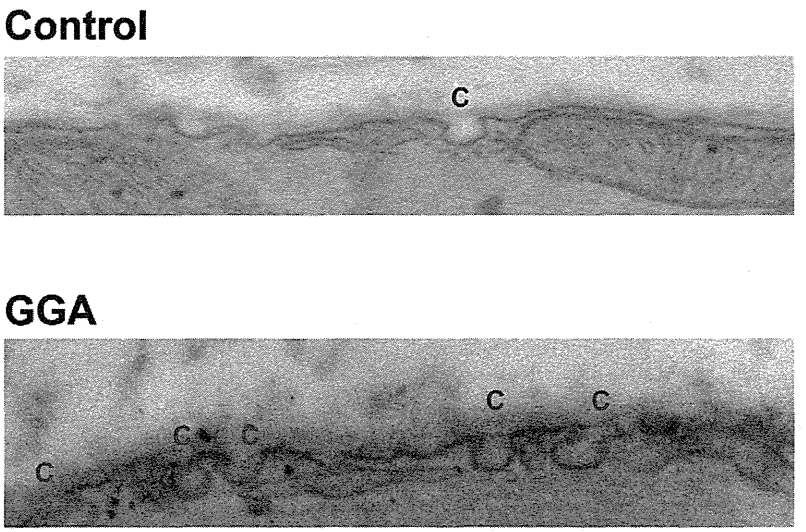

Fig. 1. Geranylgeranylacetone (GGA) increases myocardial caveolae. Electron microscopy of control and GGA treated mouse myocardium revealed a significant increase in caveolae (red C) at the sarcolemmal surface in GGA treated mice.

We found no significant differences between wild-type and Cav-3 KO mice in heart rate, blood pressure, or rate pressure product with and without GGA administration at the baseline period (Table 1). The area at risk was calculated as a percentage of the left ventricle mass and was similar between groups (Fig. 3A). Twenty-four hours after GGA administration, a significant reduction in myocardial ischemia/reperfusion injury was observed compared with vehicle control in the wild-type mice (29.0 ± 3.7% [n = 8] vs. 44.1 ± 9.3% [n = 10],

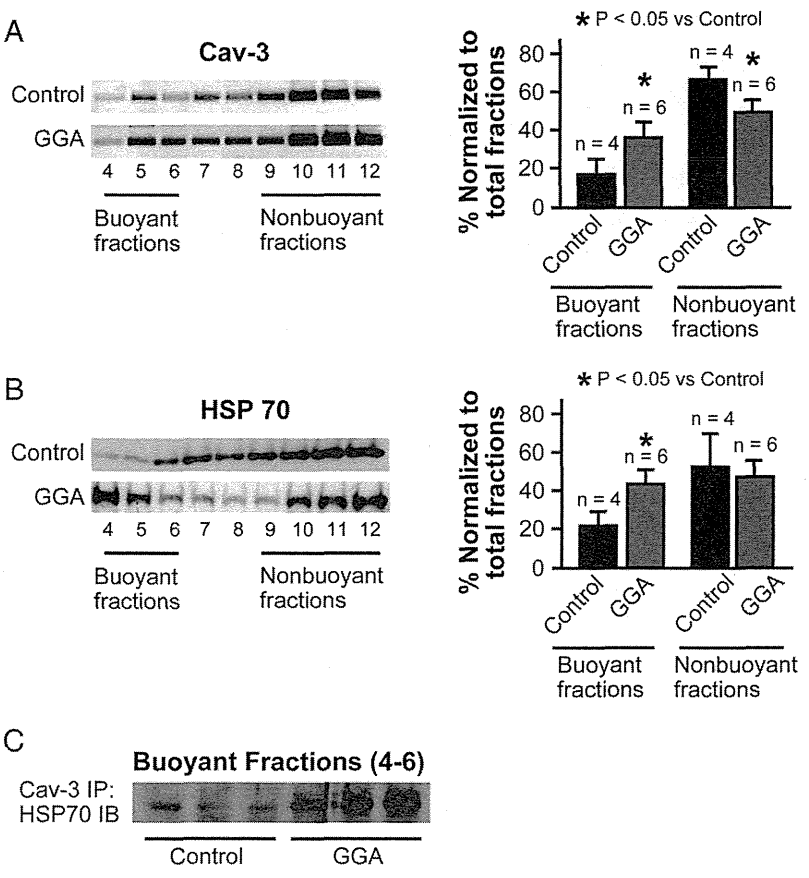

Fig. 2. Lysed and fractionated hearts on a sucrose density gradient. Fractions 4–6 were considered buoyant and 9–12 non-buoyant fractions. *P < 0.05 treated group versus control. A) and B) Fractions were collected and probed for both caveolin-3 (Cav-3) and heat shock protein 70 (HSP 70). Significant buoyant fraction localization of Cav-3 and HSP 70 was observed in geranylgeranylacetone (GGA) treated groups. C) The resulting lysates were immunoprecipitated (IP) with Cav-3 antibody and immunoblotted (IB) for HSP 70; n = 3 animals per group. There was an increased association of Cav-3 with HSP 70 after GGA administration.

Table 1
Hemodynamics parameters at baseline period.

	Control	GGA	Cav-3 KO	GGA + Cav-3 KO
Heart rate (/min)	421 ± 33	437 ± 21	413 ± 35	426 ± 37
MAP (mm Hg)	73 ± 6	69 ± 8	71 ± 4	70 ± 3
RPP (beats·min^{-1}·mm Hg·10^3)	30.5 ± 3.7	30.0 ± 3.3	29.4 ± 4.0	29.8 ± 2.3

MAP, mean arterial pressure; RPP, rate-pressure product. Data are expressed as mean ± SD.

respectively). However, in Cav-3 KO mice, this cardiac-protective effect of GGA was abolished (42.1 ± 5.2% [n = 8], Fig. 3B). Additionally, we confirmed these effects by measuring serum troponin I level, a marker of cardiac myocyte damage (Fig. 3C).

GGA reduces Ca^{2+}-induced swelling in isolated mouse heart mitochondria (Fig. 4). In wild-type mice, the addition of 100 μM Ca^{2+} caused a significant decrease in absorbance, indicating mitochondrial swelling. Ca^{2+} induced swelling was inhibited by cyclosporine A, a mPTP inhibitor, as reported previously (Tsutsumi et al., 2011). Under these conditions, GGA significantly attenuated Ca^{2+} induced swelling compared with the control; however, these effects were abolished in Cav-3 KO mice.

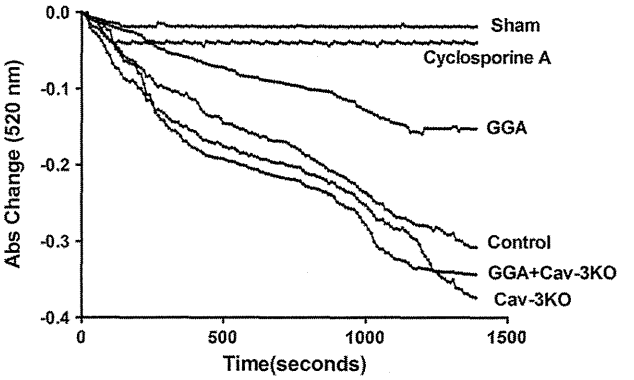

Fig. 4. Geranylgeranylacetone (GGA) inhibits mitochondrial swelling caused by ischemia-reperfusion injury. GGA treated mitochondria were isolated and revealed substantially less mitochondrial swelling compared to non-treated and Cav-3 KO mice with and without GGA when exposed to calcium chloride. Cyclosporine A was used as a control to inhibit $CaCl_2$ induced mitochondrial swelling to confirm the mitochondrial permeability transition pore (mPTP) dependence of calcium-induced swelling (n = 3).

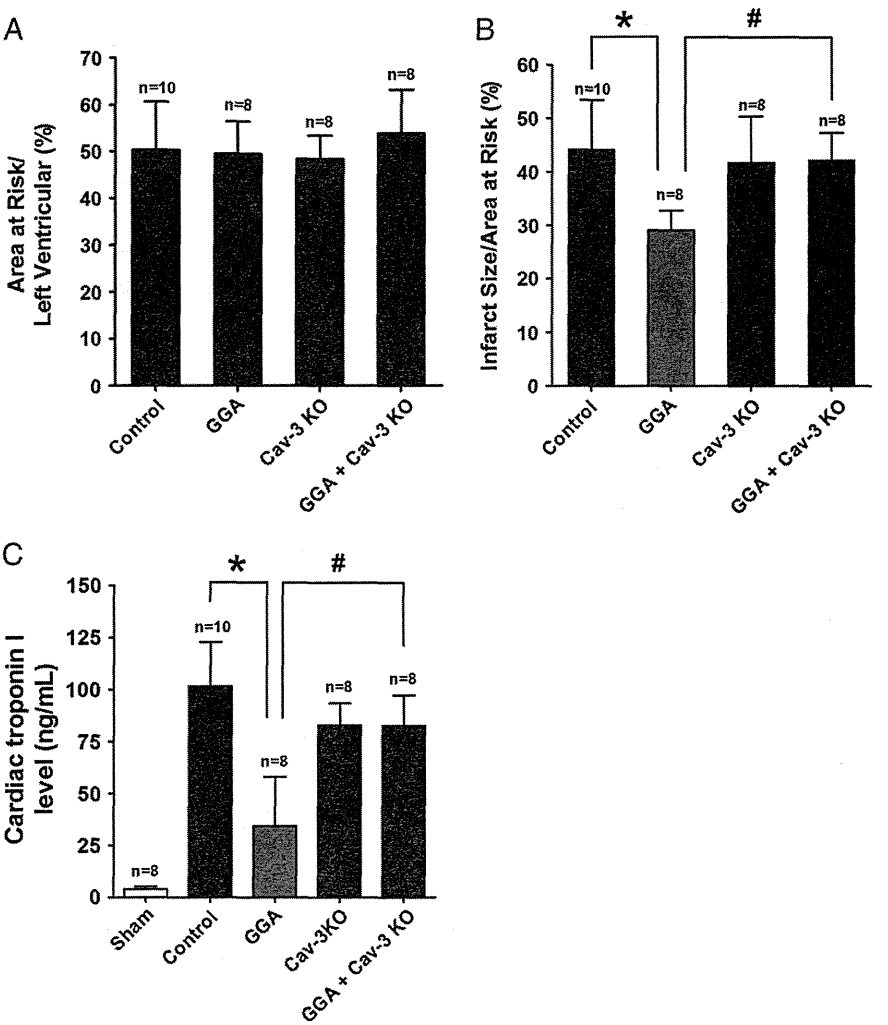

Fig. 3. Geranylgeranylacetone (GGA) protects the mouse myocardium from ischemic injury. A) Area at risk was calculated as a percentage of the left ventricle and revealed no significant differences between all groups. B) GGA was able to induce significant protection in control animals, although no protection was observed in Cav-3 KO mice. C) Cardiac troponin I, a marker of myocardial damage also revealed a significant decrease in GGA treated control mice, but no effect in Cav-3 KO mice. * $P < 0.05$; # $P < 0.05$.

Discussion

GGA, an anti-ulcer medication has been shown to have cardio-protective effects and modulate heat shock proteins, however the exact mechanisms on how this oral medication is able to enter the myocardial cell is unknown. We show that caveolae and Cav-3 are essential for GGA uptake and cardiac protection, by mediating the activation of HSP 70. Furthermore, these effects are not only mediated by caveolae and caveolins, but also directly affect mitochondrial function. These data suggest that GGA utilizes caveolae and caveolins in order to navigate the complex cell structure and facilitate protective signaling via mitochondria.

Caveolae are cholesterol and sphingolipid enriched invaginations of the plasma membrane that play a role in physiological functions and vital to cardio-protective mechanisms. In some cases, caveolae and caveolins regulate receptor stability, myocardial hypertrophy (Horikawa et al., 2011), signaling (Lisanti et al., 1994; Ostrom et al., 2001, 2002; Patel et al., 2007; Steinberg and Brunton, 2001), calcium homeostasis (Fujimoto, 1993), and endocytosis (Anderson, 1993). Recently, a decreased number of myocardial caveolae was described in Cav-3 KO mice although Cav-1 levels remained stable (Hagiwara et al., 2000; Horikawa et al., 2008; Tsutsumi et al., 2010b). Furthermore, these mice lose the ability to undergo preconditioning-like cardiac protection from ischemia/reperfusion injury (Horikawa et al., 2008). These results implicate a role for Cav-3 and the presence of caveolae in cardiac protection from ischemia/reperfusion injury. The current data show that GGA similarly requires Cav-3 and caveolae. These effects are likely due to the ability of Cav-3 and caveolae to be able to regulate mitochondrial pore activity and mediate mitochondrial mediated cell death. Furthermore, recent investigations have revealed that caveolae and caveolins can directly interact with mitochondria and regulate mitochondrial function, suggesting a potential regulatory role in surface and inter-organelle signaling (Fridolfsson et al., 2012).

In the present study, we show that the administration of GGA led to a significant increase in Cav-3 protein expression within the buoyant fraction, and that HSP 70 directly localized and interacted with Cav-3. Many previous studies using GGA have focused on HSP 70 induction (Hirakawa et al., 1996; Sakabe et al., 2008) and have suggested that GGA protects the myocardium by activating heat shock proteins especially HSP 72 (Kitahata et al., 2008; Ooie et al., 2005; Ooie et al., 2001; Yamanaka et al., 2003). Although there has been little evidence regarding the relationship between caveolae, caveolins and heat shock proteins within the heart, other organ systems including skin and cancer have investigated this relationship. In skin models, HSP have been shown to localize into caveolae, which then can regulate intracellular HSP expression (Black et al., 2011). Furthermore, in tumor cells, Cav-1 has been shown to have direct effects on HSP expression (Ciocca et al., 2012). Perhaps, in regard to GGA, caveolae are spatial hubs that localize GGA and HSP, together regulating temporal relations and activation. Given the multifaceted nature of caveolae and caveolins, multiple survival pathways are being activated simultaneously.

Glucose transporter 4 receptor (Glut4) has also been implicated in delayed preconditioning of the myocardium. Interestingly, Cav-3 KO mice are unable to be protected via isoflurane, due to its inability to translocate Glut 4, although this is preserved in Cav-1 KO, making this a Cav-3 specific phenomenon (Tsutsumi et al., 2010b). Perhaps GGA may also have effects on Glut4 translocation and expression.

There are several limitations in the present study. First, we evaluated the effects of Cav-3 and HSP 70 in experiments that investigated ischemia/reperfusion injury. GGA induces a broad class of the protective proteins, including various families of HSPs (Brundel et al., 2006a, 2006b), protein kinase C (Yamanaka et al., 2003), and nitric oxide (Yamamoto et al., 2005). Second, the dose and time period used for cardiac protection in mice are unknown. Previous studies have all been in rats, where a single oral dose of 200 mg/kg GGA induced HSP and cardiac protection against ischemia/reperfusion (Ooie et al., 2005, 2001; Shinohara et al., 2007; Yamanaka et al., 2003). The same concentration and dose were applied in this study.

Taken together these data demonstrate that GGA had delayed cardio-protective effects that are dependent on caveolae and Cav-3. We show that caveolae and Cav-3 are the vital conduits between HSP-70 activation and subsequent mitochondrial respiration suggesting an important role for this structural protein. Furthermore, these data suggest that GGA may be a unique way to clinically increase caveolae and caveolin-3 expression, which have both shown to have significant cardioprotective effects against ischemic injury and detrimental remodeling.

Conflict of interest statement

The authors declare that there are no conflicts of interest.

Acknowledgments

Supported by JSPS KAKENHI Numbers 23592994, 24592300, 25462404, and 25462405 from Japan Society for the Promotion of Science, Tokyo.

References

Anderson RG. Potocytosis of small molecules and ions by caveolae. Trends Cell Biol 1993; 3:69–72.
Black AT, Hayden PJ, Casillas RP, Heck DE, Gerecke DR, Sinko PJ, et al. Regulation of Hsp27 and Hsp70 expression in human and mouse skin construct models by caveolae following exposure to the model sulfur mustard vesicant, 2-chloroethyl ethyl sulfide. Toxicol Appl Pharmacol 2011;253:112–20.
Brundel BJ, Henning RH, Ke L, van Gelder IC, Crijns HJ, Kampinga HH. Heat shock protein upregulation protects against pacing-induced myolysis in HL-1 atrial myocytes and in human atrial fibrillation. J Mol Cell Cardiol 2006a;41:555–62.
Brundel BJ, Shiroshita-Takeshita A, Qi X, Yeh YH, Chartier D, van Gelder IC, et al. Induction of heat shock response protects the heart against atrial fibrillation. Circ Res 2006b;99: 1394–402.
Ciocca DR, Cuello-Carrion FD, Natoli AL, Restall C, Anderson RL. Absence of caveolin-1 alters heat shock protein expression in spontaneous mammary tumors driven by Her-2/neu expression. Histochem Cell Biol 2012;137:187–94.
Fridolfsson HN, Kawaraguchi Y, Ali SS, Panneerselvam M, Niesman IR, Finley JC, et al. Mitochondria-localized caveolin in adaptation to cellular stress and injury. FASEB J 2012;26:4637–49.
Fujimoto T. Calcium pump of the plasma membrane is localized in caveolae. J Cell Biol 1993;120:1147–57.
Fujimoto M, Yamanaka T, Bessho M, Igarashi T. Effects of geranylgeranylacetone on gastrointestinal secretion in rats. Eur J Pharmacol 1982;77:113–8.
Hagiwara Y, Sasaoka T, Araishi K, Imamura M, Yorifuji H, Nonaka I, et al. Caveolin-3 deficiency causes muscle degeneration in mice. Hum Mol Genet 2000;9:3047–54.
Hirakawa T, Rokutan K, Nikawa T, Kishi K. Geranylgeranylacetone induces heat shock proteins in cultured guinea pig gastric mucosal cells and rat gastric mucosa. Gastroenterology 1996;111:345–57.
Hirose K, Tsutsumi YM, Tsutsumi R, Shono M, Katayama E, Kinoshita M, et al. Role of the O-linked beta-N-acetylglucosamine in the cardioprotection induced by isoflurane. Anesthesiology 2011;115:955–62.
Horikawa YT, Patel HH, Tsutsumi YM, Jennings MM, Kidd MW, Hagiwara Y, et al. Caveolin-3 expression and caveolae are required for isoflurane-induced cardiac protection from hypoxia and ischemia/reperfusion injury. J Mol Cell Cardiol 2008;44: 123–30.
Horikawa YT, Panneerselvam M, Kawaraguchi Y, Tsutsumi YM, Ali SS, Balijepalli RC, et al. Cardiac-specific overexpression of caveolin-3 attenuates cardiac hypertrophy and increases natriuretic peptide expression and signaling. J Am Coll Cardiol 2011;57: 2273–83.
Kitahata H, Nozaki J, Kawahito S, Tomino T, Oshita S. Low-dose sevoflurane inhalation enhances late cardioprotection from the anti-ulcer drug geranylgeranylacetone. Anesth Analg 2008;107:755–61.
Lisanti MP, Scherer PE, Tang Z, Sargiacomo M. Caveolae, caveolin and caveolin-rich membrane domains: a signalling hypothesis. Trends Cell Biol 1994;4:231–5.
Murakami M, Oketani K, Fujisaki H, Wakabayashi T, Ohgo T. Antiulcer effect of geranylgeranylacetone, a new acyclic polyisoprenoid on experimentally induced gastric and duodenal ulcers in rats. Arzneimittelforschung 1981;31:799–804.
Ooie T, Takahashi N, Saikawa T, Nawata T, Arikawa M, Yamanaka K, et al. Single oral dose of geranylgeranylacetone induces heat-shock protein 72 and renders protection against ischemia/reperfusion injury in rat heart. Circulation 2001;104: 1837–43.
Ooie T, Kajimoto M, Takahashi N, Shinohara T, Taniguchi Y, Kouno H, et al. Effects of insulin resistance on geranylgeranylacetone-induced expression of heat shock protein 72 and cardioprotection in high-fat diet rats. Life Sci 2005;77:869–81.
Ostrom RS, Gregorian C, Drenan RM, Xiang Y, Regan JW, Insel PA. Receptor number and caveolar co-localization determine receptor coupling efficiency to adenylyl cyclase. J Biol Chem 2001;276:42063–9.

Ostrom RS, Liu X, Head BP, Gregorian C, Seasholtz TM, Insel PA. Localization of adenylyl cyclase isoforms and G protein-coupled receptors in vascular smooth muscle cells: expression in caveolin-rich and noncaveolin domains. Mol Pharmacol 2002;62: 983–92.

Palade G. Fine structure of blood capillaries. J Appl Phys 1953;24:1424–36.

Patel HH, Tsutsumi YM, Head BP, Niesman IR, Jennings M, Horikawa Y, et al. Mechanisms of cardiac protection from ischemia/reperfusion injury: a role for caveolae and caveolin-1. FASEB J 2007;21:1565–74.

Patel HH, Murray F, Insel PA. Caveolae as organizers of pharmacologically relevant signal transduction molecules. Annu Rev Pharmacol Toxicol 2008;48: 359–91.

Sakabe M, Shiroshita-Takeshita A, Maguy A, Brundel BJ, Fujiki A, Inoue H, et al. Effects of a heat shock protein inducer on the atrial fibrillation substrate caused by acute atrial ischaemia. Cardiovasc Res 2008;78:63–70.

Shinohara T, Takahashi N, Kohno H, Yamanaka K, Ooie T, Wakisaka O, et al. Mitochondria are targets for geranylgeranylacetone-induced cardioprotection against ischemia–reperfusion in the rat heart. Am J Physiol Heart Circ Physiol 2007;293: H1892–9.

Steinberg SF, Brunton LL. Compartmentation of G protein-coupled signaling pathways in cardiac myocytes. Annu Rev Pharmacol Toxicol 2001;41:751–73.

Tsutsumi YM, Patel HH, Lai NC, Takahashi T, Head BP, Roth DM. Isoflurane produces sustained cardiac protection after ischemia–reperfusion injury in mice. Anesthesiology 2006;104:495–502.

Tsutsumi YM, Yokoyama T, Horikawa Y, Roth DM, Patel HH. Reactive oxygen species trigger ischemic and pharmacological postconditioning: in vivo and in vitro characterization. Life Sci 2007;81:1223–7.

Tsutsumi YM, Horikawa YT, Jennings MM, Kidd MW, Niesman IR, Yokoyama U, et al. Cardiac-specific overexpression of caveolin-3 induces endogenous cardiac protection by mimicking ischemic preconditioning. Circulation 2008;118:1979–88.

Tsutsumi YM, Kawaraguchi Y, Horikawa YT, Niesman IR, Kidd MW, Chin-Lee B, et al. Role of caveolin-3 and glucose transporter-4 in isoflurane-induced delayed cardiac protection. Anesthesiology 2010a;112:1136–45.

Tsutsumi YM, Kawaraguchi Y, Niesman IR, Patel HH, Roth DM. Opioid-induced preconditioning is dependent on caveolin-3 expression. Anesth Analg 2010b;111:1117–21.

Tsutsumi YM, Tsutsumi R, Mawatari K, Nakaya Y, Kinoshita M, Tanaka K, et al. Compound K, a metabolite of ginsenosides, induces cardiac protection mediated nitric oxide via Akt/PI3K pathway. Life Sci 2011;88:725–9.

Yamamoto K, Sarukawa M, Ito T, Aoki H, Ichida M, Shimada K. An anti-ulcer drug, geranylgeranylacetone, suppresses inducible nitric oxide synthase in cultured vascular smooth muscle cells. J Hypertens 2005;23:1847–53.

Yamanaka K, Takahashi N, Ooie T, Kaneda K, Yoshimatsu H, Saikawa T. Role of protein kinase C in geranylgeranylacetone-induced expression of heat-shock protein 72 and cardioprotection in the rat heart. J Mol Cell Cardiol 2003;35:785–94.

Zhu Z, Takahashi N, Ooie T, Shinohara T, Yamanaka K, Saikawa T. Oral administration of geranylgeranylacetone blunts the endothelial dysfunction induced by ischemia and reperfusion in the rat heart. J Cardiovasc Pharmacol 2005;45:555–62.

Epac1-dependent phospholamban phosphorylation mediates the cardiac response to stresses

Satoshi Okumura,[1,2] Takayuki Fujita,[1] Wenqian Cai,[1] Meihua Jin,[1] Iyuki Namekata,[3] Yasumasa Mototani,[2] Huiling Jin,[1] Yoshiki Ohnuki,[2] Yayoi Tsuneoka,[3] Reiko Kurotani,[1,4] Kenji Suita,[1] Yuko Kawakami,[3] Shogo Hamaguchi,[3] Takaya Abe,[5] Hiroshi Kiyonari,[5] Takashi Tsunematsu,[1,6] Yunzhe Bai,[1] Sayaka Suzuki,[1] Yuko Hidaka,[1] Masanari Umemura,[1] Yasuhiro Ichikawa,[1] Utako Yokoyama,[1] Motohiko Sato,[1,7] Fumio Ishikawa,[8] Hiroko Izumi-Nakaseko,[9] Satomi Adachi-Akahane,[10] Hikaru Tanaka,[3] and Yoshihiro Ishikawa[1]

[1]Cardiovascular Research Institute, Yokohama City University Graduate School of Medicine, Yokohama, Japan. [2]Department of Physiology, Tsurumi University School of Dental Medicine, Yokohama, Japan. [3]Department of Pharmacology, Faculty of Pharmaceutical Sciences, Toho University, Chiba, Japan. [4]Biochemical Engineering, Faculty of Engineering, Yamagata University, Yamagata, Japan. [5]Laboratory for Animal Resources and Genetic Engineering, RIKEN Center for Developmental Biology, Kobe, Japan. [6]Department of Medicine (Cardiology), Atami Hospital, International University of Health and Welfare, Shizuoka, Japan. [7]Department of Physiology, Aichi Medical University, Aichi, Japan. [8]Department of Immunology, [9]Department of Pharmacology, and [10]Department of Physiology, School of Medicine, Faculty of Medicine, Toho University, Tokyo, Japan.

PKA phosphorylates multiple molecules involved in calcium (Ca^{2+}) handling in cardiac myocytes and is considered to be the predominant regulator of β-adrenergic receptor–mediated enhancement of cardiac contractility; however, recent identification of exchange protein activated by cAMP (EPAC), which is independently activated by cAMP, has challenged this paradigm. Mice lacking *Epac1* (*Epac1* KO) exhibited decreased cardiac contractility with reduced phospholamban (PLN) phosphorylation at serine-16, the major PKA-mediated phosphorylation site. In *Epac1* KO mice, intracellular Ca^{2+} storage and the magnitude of Ca^{2+} movement were decreased; however, PKA expression remained unchanged, and activation of PKA with isoproterenol improved cardiac contractility. In contrast, direct activation of EPAC in cardiomyocytes led to increased PLN phosphorylation at serine-16, which was dependent on PLC and PKCε. Importantly, *Epac1* deletion protected the heart from various stresses, while *Epac2* deletion was not protective. Compared with WT mice, aortic banding induced a similar degree of cardiac hypertrophy in *Epac1* KO; however, lack of *Epac1* prevented subsequent cardiac dysfunction as a result of decreased cardiac myocyte apoptosis and fibrosis. Similarly, *Epac1* KO animals showed resistance to isoproterenol- and aging-induced cardiomyopathy and attenuation of arrhythmogenic activity. These data support *Epac1* as an important regulator of PKA-independent PLN phosphorylation and indicate that *Epac1* regulates cardiac responsiveness to various stresses.

Introduction

β-Adrenergic receptor (β-AR) signaling is well established as a primary defense mechanism against acute stress or changes in hemodynamic load; however, its role in cardiac pathogenesis, although studied extensively, remains poorly understood (1). β-AR blockade, rather than stimulation, is beneficial in patients with heart failure, and pharmacological inhibition of the entire β-AR signaling pathway at the receptor level is one of the accepted treatments for heart failure (2). Studies in mouse models overexpressing β-AR, Gsα, or PKA support the usefulness of β-AR blockade in heart failure (3–5). Recently, however, we have developed a mouse model in which type 5 adenylyl cyclase (AC), a major cardiac subtype, is disrupted (*Ac5* KO), and we found that *Ac5* KO showed resistance to the development of heart failure and exhibited increased longevity (6–9), indicating that inhibition of cAMP signaling at the level of AC, not β-AR, may also result in cardiac protection.

Systolic contraction follows activation of sarcolemmal voltage-gated L-type calcium (Ca^{2+}) channel during an action potential, resulting in Ca^{2+}-influx, which activates cardiac ryanodine receptor (RyR2) Ca^{2+} release channels on the sarcoplastic reticulum (SR) (major intracellular Ca^{2+} store). Diastolic relaxation occurs with cessation of Ca^{2+} release, and Ca^{2+} sequestration by the SR Ca^{2+}-transporting adenosine triphosphatase (SERCA2a) and its regulator, phospholamban (PLN), indicate that phosphorylations of PLN and RyR2 have a central role in modulating Ca^{2+} homeostasis and, therefore, cardiac function (10, 11). PLN is a low-molecular weight phosphoprotein in cardiac SR, and dephosphorylated PLN is an inhibitor of SERCA2a-mediated transport of Ca^{2+}. Following β-AR activation, and thus production of cAMP by AC, PKA phosphorylates PLN on serine-16 (10) in addition to RyR2 on serine-2808 and serine-2814 (11). PKA-mediated serine-16 phosphorylation (and thus SERCA2a activation) is the major mechanism of the lusitropic and also inotropic (12) effects of β-AR stimulation in regulating cardiac function (13). In failing hearts, in contrast, decreased PLN phosphorylation, and thus a decrease in Ca^{2+} uptake by SERCA2a, is a central feature (14, 15). Indeed, decreased inhibition of SERCA2a by PLN ablation can prevent progression of heart failure (16, 17).

Authorship note: Satoshi Okumura, Takayuki Fujita, Wenqian Cai, and Meihua Jin contributed equally to this work.

Conflict of interest: The authors have declared that no conflict of interest exists.

Citation for this article: *J Clin Invest.* 2014;124(6):2785–2801. doi:10.1172/JCI64784.

Table 1
Heart size and cardiac function in *Epac1* KO

	WT (*n*)	*Epac1* KO (*n*)
Age, month	4.2 ± 0.1 (32)	4.2 ± 0.2 (21)
BW, g	30 ± 0.7 (21)	29 ± 0.9 (18)
Tibia, mm	17.5 ± 0.1 (21)	17.4 ± 0.1 (18)
LV/tibia (mg/mm)	5.2 ± 0.2 (20)	5.2 ± 0.2 (18)
LV/BW (mg/g)	3.2 ± 0.1 (20)	3.3 ± 0.2 (18)
LVEDD, mm	4.3 ± 0.03 (31)	4.4 ± 0.1 (18)
LVESD, mm	2.9 ± 0.04(31)	3.3 ± 0.1 (18)[A]
LVEF, %	70 ± 0.8 (31)	60 ± 1.1 (18)[A]
%FS	35 ± 1.1 (31)	26 ± 0.6 (18)[A]
Max dP/dt, mmHg	9091 ± 240 (17)	7246 ± 226 (16)[A]
Min dP/dt, mmHg	−9110 ± 240 (18)	−6201 ± 125 (14)[A]

Data are mean ± SEM. LVEDD, LV end-diastolic diameter. FS, fractional shortening. [A]$P < 0.01$.

Others have found that decreased inhibition of SERCA2a through PLN ablation or hyperphosphorylation of PLN exaggerated heart failure and arrhythmogenic activity (18–22). Thus, it remains controversial whether or not enhancement of Ca^{2+} uptake through PLN ablation or PLN hyperphosphorylation can inhibit the progression of heart failure. Nevertheless, it is well accepted that β-AR–mediated phosphorylation of PLN plays a central role in regulating cardiac function and also in the pathogenesis of cardiac failure.

But PKA is not the only molecule activated by cAMP. Exchange protein activated by cAMP (EPAC) was recently identified as a new target of cAMP signaling that is activated independently of PKA (23, 24). EPAC has 2 isoforms (*Epac1* and *Epac2*), and *Epac1* is predominantly expressed in the heart. EPAC modulates various cellular functions, including migration, proliferation, exocytosis, and apoptosis, via regulation of RAP1 (25). In cardiac myocytes, EPAC activation induced hypertrophy (26). In adult mouse cardiac myocytes, pharmacological EPAC activation with an EPAC-selective but not isoform-selective cAMP analogue was reported to enhance evoked Ca^{2+} transients through the PLCε/PKCε/CaMKII pathway, and activation of CaMKII via EPAC induced store depletion and enhancement of Ca^{2+} sparks through increased phosphorylation of PLN on threonine-17 and RyR2 on serine-2815 by EPAC via phospholipase C (PLC) ε/PKC ε/Ca^{2+}/calmodulin-dependent protein kinase II (CaMKII) (27–29). EPAC2 was also reported to be closely associated with CaMKII, and EPAC2 mediated β_1-AR–induced cardiac arrhythmia via CaMKIIδ (a major isoform of cardiac CaMKII) and RyR2 phosphorylation on serine-2815 (30). However, the isoform-specific role of EPAC in cardiac function and pathogenesis remains poorly understood.

Here, we show that EPAC1, in an additive and independent manner with respect to PKA, phosphorylates PLN and RyR2 to regulate cardiac function. Loss of EPAC1 slightly decreased basal cardiac function, but afforded greater protection against various stresses, including arrhythmogenic stress, whereas loss of EPAC2 did not show cardioprotective effects. Accordingly, selective EPAC1 inhibition may prevent hyperphosphorylation of PLN and RyR2, and this may be an alternative strategy to current β-AR blocker therapy for the treatment of established cardiac failure or arrhythmia.

Results

Cardiac function is decreased in Epac1 KO. Because EPAC activation induced cardiac myocyte hypertrophy in culture (26), we originally thought that EPAC might play a role in regulating cardiac myocyte growth. Therefore, we genetically disrupted *Epac1* in mice (*Epac1* KO) (31), but found that these mice did not show any change in the size of the heart. Instead, *Epac1* KO exhibited a modest, but significant, decrease in cardiac function. LV ejection fraction (LVEF) was significantly decreased (WT versus *Epac1* KO: 70% ± 0.8% versus 60% ± 1.1%, n = 18–31, $P < 0.01$), and LV end-systolic diameter (LVESD) was increased (WT versus *Epac1* KO: 4.3 ± 0.03 versus 4.4 ± 0.1 mm, n = 18–31, $P < 0.01$) (Table 1). Hemodynamic measurements demonstrated that Max dP/dt was significantly decreased (WT versus *Epac1* KO: 9091 ± 240 versus 7246 ± 226 mmHg, n = 16–17, $P < 0.01$), and Min dP/dt was significantly increased in *Epac1* KO (WT versus *Epac1* KO: −9110 ± 240 versus −6201 ± 125 mmHg, n = 14–18, $P < 0.01$) (Table 1). Because disruption of *Epac1* might alter the expression of other molecules involved in cAMP signaling, such as PKA subunits, we examined the protein expression of β_1-AR, β_2-AR, β-AR kinase (βARK), Gsα, Giα, Gβ, Gq, and type 5/6 AC in addition to PKA subunits by means of Western blotting (Supplemental Figure 1A; supplemental material available online with this article; doi:10.1172/JCI64784DS1). There was no difference in expression of these molecules between WT and *Epac1* KO. Also, there was no compensatory increase of *Epac2* isoform in *Epac1* KO at either the mRNA or protein level (Supplemental Figure 1, A and B).

Decreased cardiac function in *Epac1* KO was readily compensated by isoproterenol (ISO) infusion. Responses of LVEF and LVESD to ISO (0, 0.13, 0.27, 0.40 μg/kg/min for 5 minutes) were well preserved and, indeed, reached the same level as those of WT (Supplemental Figure 2, A and B). Changes in cardiac contractility were further examined using isolated segments of myocardium (Supplemental Figure 3). The basal contractile force was significantly smaller in *Epac1* KO (WT versus *Epac1* KO: 112 ± 14.7 versus 73 ± 7.1 mg/mm^2, n = 6–7, $P < 0.05$) (Supplemental Figure 3A). ISO dose dependently enhanced the contractile force in WT and *Epac1* KO. The magnitude of increase in response to ISO was similar in WT and *Epac1* KO (Supplemental Figure 3B). The sensitivity to β-adrenergic stimulation with ISO as represented by the -log EC_{50} value for the enhancement of contractile force was 7.04 ± 0.07 in WT and 7.06 ± 0.01 in *Epac1* KO (P = NS, n = 6–7). The time required to reach peak tension was also similar in *Epac1* KO and WT at baseline (WT versus *Epac1* KO: 50 ± 1.1 versus 52 ± 1.5 ms, n = 6–7, P = NS) and decreased similarly in both WT and *Epac1* KO (Supplemental Figure 3C). However, the time required for 90% relaxation was significantly longer in *Epac1* KO at baseline (WT versus *Epac1* KO: 54 ± 1.5 versus 61 ± 2.0 ms, n = 6–7, $P < 0.05$), but became similar in response to ISO (Supplemental Figure 3D). Thus, *Epac1* KO showed decreased cardiac function, exemplified most clearly by delayed relaxation, but the dysfunction was readily compensated by β-AR stimulation.

PLN phosphorylation on serine-16 is decreased in Epac1 KO. Phosphorylation of PLN occurs, following β-adrenergic stimulation, on serine-16 and threonine-17. Indeed, PKA-mediated serine-16 phosphorylation is a key event in increasing cardiac function (32). Unexpectedly, phosphorylation on serine-16 was significantly decreased in *Epac1* KO (WT versus *Epac1* KO: 100% ± 6.5% versus 57% ± 7.1%, n = 6, $P < 0.01$) (Figure 1A) despite the absence of any difference in expression of the PKA catalytic and regulatory units (RIα, RIIα) (Supplemental Figure 1A). PLN phosphorylation on threonine-17 (Figure 1B), which is mediated by CaMKII, was similar in WT and *Epac1* KO. Phosphorylation on threonine-286, and thus activation of CaMKII, was also similar (Supplemental Figure 4).

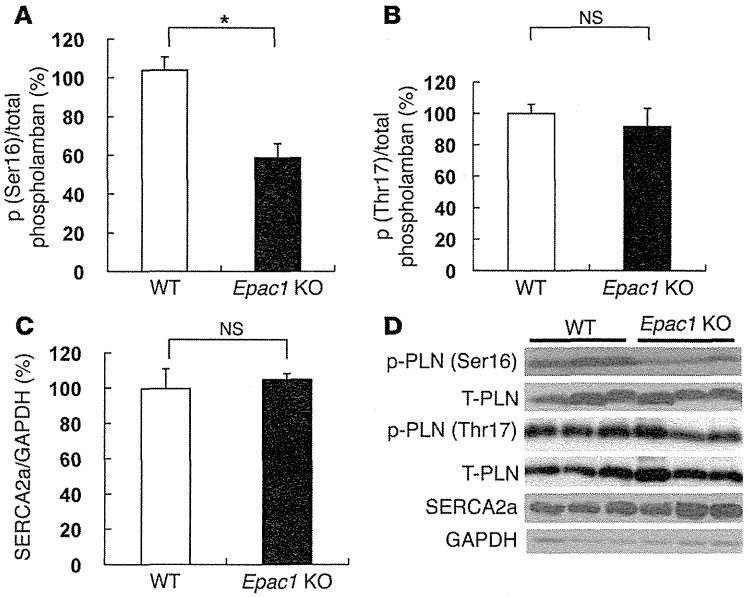

Figure 1
Phosphorylation of PLN on serine-16 and threonine-17 and SERCA2a expression in the heart of *Epac1* KO at baseline. (**A**) Phosphorylation on serine-16 (Ser16) was significantly decreased in *Epac1* KO compared with WT (WT versus *Epac1* KO: 100% ± 6.5% versus 57% ± 7.1%, $n = 6$, $^*P < 0.01$). The ratio of phosphorylated/total protein expression of PLN in WT was taken as 100% in each determination. (**B**) Phosphorylation on threonine-17 (Thr17) was not different in *Epac1* KO and WT (WT versus *Epac1* KO: 100% ± 5.7% versus 92% ± 11.5%, $n = 7–10$, P = NS). The ratio of phosphorylated/total protein expression of PLN in WT was taken as 100% in each determination. (**C**) The expression of SERCA2a protein was not different in WT and *Epac1* KO at baseline (WT versus *Epac1* KO: 100% ± 11.1% versus 105% ± 3.5%, $n = 6–7$, P = NS). The ratio of SERCA2a protein/GAPDH in WT was taken as 100% in each determination. (**D**) Representative immunoblotting results of phosphorylation of PLN on serine-16 (upper) and threonine-17 (middle) and SERCA2a (lower) are shown. T-PLN, total PLN; p-PLN, phosphorylated PLN.

EPAC-selective cAMP analogue increases PLN phosphorylation on serine-16 and threonine-17 in neonatal rat cardiac myocytes. The above findings indicated that disruption of EPAC, but not PKA, decreased PLN phosphorylation. When we examined the consequences of EPAC activation for PLN phosphorylation in neonatal rat cardiac myocytes, we used a new membrane-permeable EPAC-selective but not isoform-selective agonist, i.e., 8-(4-chlorophenylthio)-2′-O-Me-cAMP-AM (8-CPT-AM) (33). We found that 10 μM 8-CPT-AM was necessary to obtain a significant PLN phosphorylation signal with our detection system in neonatal rat cardiac myocytes (Figure 2D), and thus this concentration was used. This concentration of 8-CPT-AM is in line with those used in previous studies to examine EPAC-mediated signaling, i.e., 10 μM for adult rat cardiac myocytes (34) or 50 μM for 293T, JAR, and BeWo cells (35). Furthermore, Brette et al. reported very recently that 8-CPT-AM at 10 μM did not exert an inhibitory effect on phosphodiesterase (PDE) activity (34). On the other hand, non-AM ester 8-CPT (8-CPT) does inhibit PDE, which is undesirable, since we wish to examine EPAC-specific effects (36, 37).

We found that 8-CPT-AM significantly increased the PLN phosphorylation on serine-16 by approximately 89-fold from baseline and that on threonine-17 by approximately 19-fold from baseline at 15 minutes after the treatment with 8-CPT-AM ($n = 4$, $P < 0.01$) (Figure 2, A and B). PLN phosphorylation on serine-16 was decreased gradually, but was significantly increased even at 120 minutes after 8-CPT-AM treatment. However, PLN phosphorylation on threonine-17 decreased rapidly and did not show a significant increase at 60 minutes after 8-CPT-AM treatment. Thus, activation of EPAC with 8-CPT-AM, in addition to PKA and CaMKII, could induce PLN phosphorylation on serine-16 and threonine-17, but PLN phosphorylation on serine-16 persists for a long time, compared with that on threonine-17, which has been reported to be phosphorylated by EPAC via PLCε/PKCε/CaMKII (27, 28).

Increase of PLN phosphorylation at serine-16 was attenuated in neonatal cardiac myocytes prepared from Epac1 KO after the treatment of 8-CPT-AM. We examined the effects of 8-CPT-AM on PLN phosphorylation at serine-16 using neonatal cardiac myocytes prepared from *Epac1* KO and WT. In WT neonatal mouse cardiac myocytes, we found that 1 μM 8-CPT-AM was sufficient to obtain a significant PLN phosphorylation signal with our detection system (Supplemental Figure 5). Since the magnitude of the increase was similar to that obtained with 10 μM 8-CPT-AM in neonatal rat cardiac myocytes, we used this concentration (1 μM) (Figure 2D and Supplemental Figure 5). Epac activation with 8-CPT-AM (1 μM) significantly increased PLN phosphorylation at serine-16 from baseline in WT, and the level was also significantly greater than that in *Epac1* KO ($P < 0.05$). In contrast with WT, the increase of PLN phosphorylation at serine-16 was not significant (WT: from 100% ± 11% to 1534% ± 528%, $n = 4–6$, $P < 0.01$; *Epac1* KO: from 61% ± 22% to 476% ± 141%, $n = 4–6$, P = NS). These results, together with the data shown in Figure 1A and Figure 2A, indicate that EPAC1 is an important regulator of PLN phosphorylation at serine-16, independently of PKA. More importantly, these findings also suggest that 8-CPT-AM at the concentration of 1 μM phosphorylates PLN at serine-16 via EPAC, not other signaling pathways, such as PKA, cGMP-dependent PKG, or PDE (34, 38).

EPAC phosphorylates PLN at serine-16 via PLC/PKCε. It is established that PKC phosphorylates PLN and that the phosphorylation via PKC is additive to that via PKA and CaMKII, but the significance of these findings and the mechanisms involved remain poorly understood (39–41). It has been suggested that EPAC mediates a novel pathway of regulatory crosstalk between the cAMP and the PLC/PKC pathways (42), and so we hypothesized that EPAC mediates PLN phosphorylation on serine-16 via PLC/PKC. Indeed, in the presence of PLC inhibitor (U73122) or PKC inhibitor (Ro-31-7549), EPAC-mediated phosphorylation of serine-16 was negated in neonatal mouse and rat cardiac myocytes (Supplemental Figure 6). Twelve PKC isoforms are known to exist; conventional PKC subtypes, which include PKCα, PKCβ, and PKCγ, require both Ca^{2+} and phospholipid for activation, whereas novel PKC subtypes, which include PKCδ and PKCε, require phospholipid, but not Ca^{2+} (43). We examined the effect of silencing each

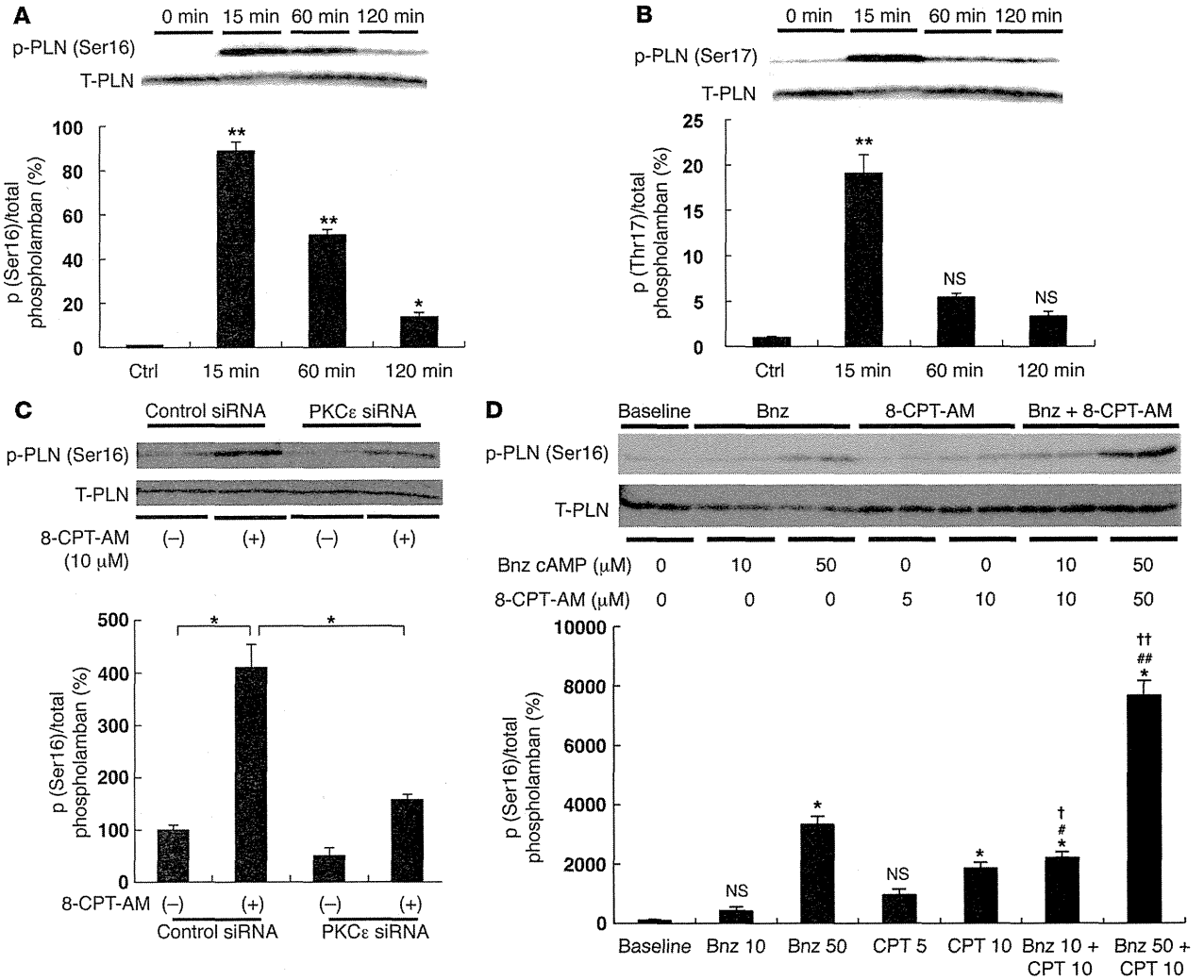

Figure 2

Effects of EPAC activation on PLN phosphorylation in neonatal rat cardiac myocytes. (**A** and **B**) *Treatment of neonatal rat cardiac myocytes with* 8-CPT-AM (10 μM). PLN phosphorylation on serine-16 was significantly increased at 15 minutes and remained significantly (*$P < 0.05$ or **$P < 0.01$ versus 0 minutes, $n = 4$) greater at 120 minutes than at 0 minutes (**A**). PLN phosphorylation on threonine-17 was also significantly increased at 15 minutes after treatment. However, increase fell below significance at 60 minutes versus 0 minutes and remained unchanged at 120 minutes (P = NS, versus 0 minutes, $n = 4$) (**B**). Ratio of phosphorylated/total protein expression of PLN at baseline (0 min: Ctrl) was taken as 1-fold. (**C**) EPAC-mediated PLN phosphorylation on serine-16 was examined in neonatal rat cardiac myocytes transfected with PKCε siRNA or control siRNA (*$P < 0.01$, $n = 5–7$). Ratio of phosphorylated/total protein expression of PLN in cells transfected with control siRNA at baseline was taken as 100%. (**D**) PLN phosphorylation on serine-16 was examined in cells treated with Bnz-cAMP (50 μM) and/or 8-CPT-AM (10 μM). (##$P < 0.001$ versus Bnz-cAMP [50 μM] alone; ††$P < 0.001$ versus 8-CPT-AM [10 μM] alone). A similar tendency was observed when 10 μM Bnz-cAMP and 5 μM 8-CPT-AM were used together (#$P < 0.001$ versus Bnz-cAMP [10 μM] alone; †$P < 0.001$ versus 8-CPT-AM [5 μM] alone, $n = 4–8$; *$P < 0.01$ versus baseline, $n = 4–8$). Ratio of phosphorylated/total protein expression of PLN at baseline was taken as 100%.

PKC isoform with siRNA on PLN phosphorylation (Supplemental Figure 7A). Silencing of PKCα, PKCβ, PKCγ, and PKCδ did not affect the EPAC-mediated PLN phosphorylation on serine-16 with 8-CPT-AM (Supplemental Figure 8). However, when PKCε was silenced with siRNA (its specificity was confirmed: Supplemental Figure 7B), EPAC-mediated PLN phosphorylation on serine-16 was significantly attenuated compared with the control (control siRNA versus PKCε siRNA: 410% ± 44% versus 158% ± 10%, $n = 5–7$, $P < 0.01$), suggesting that PKCε plays a role in PLN phosphorylation on serine-16 by EPAC (Figure 2C).

EPAC phosphorylates PLN in an additive and independent manner with respect to PKA. In order to compare the roles of EPAC and PKA in PLN phosphorylation, we examined the effects of N^6-benzoyladenosine-cAMP (Bnz-cAMP), a PKA-selective cAMP analogue, and 8-CPT-AM, an EPAC-selective analogue (Figure 2D). The degree of PLN phosphorylation achieved with 8-CPT-AM (10 μM) was approximately 60% of that achieved with Bnz-cAMP (50 μM) (Bnz-cAMP versus 8-CPT-AM: 3324% ± 289% versus 1851% ± 202%, $n = 4–8$, $P < 0.001$). However, when 8-CPT-AM and Bnz-cAMP were used together, PLN phosphorylation was additively and significantly increased

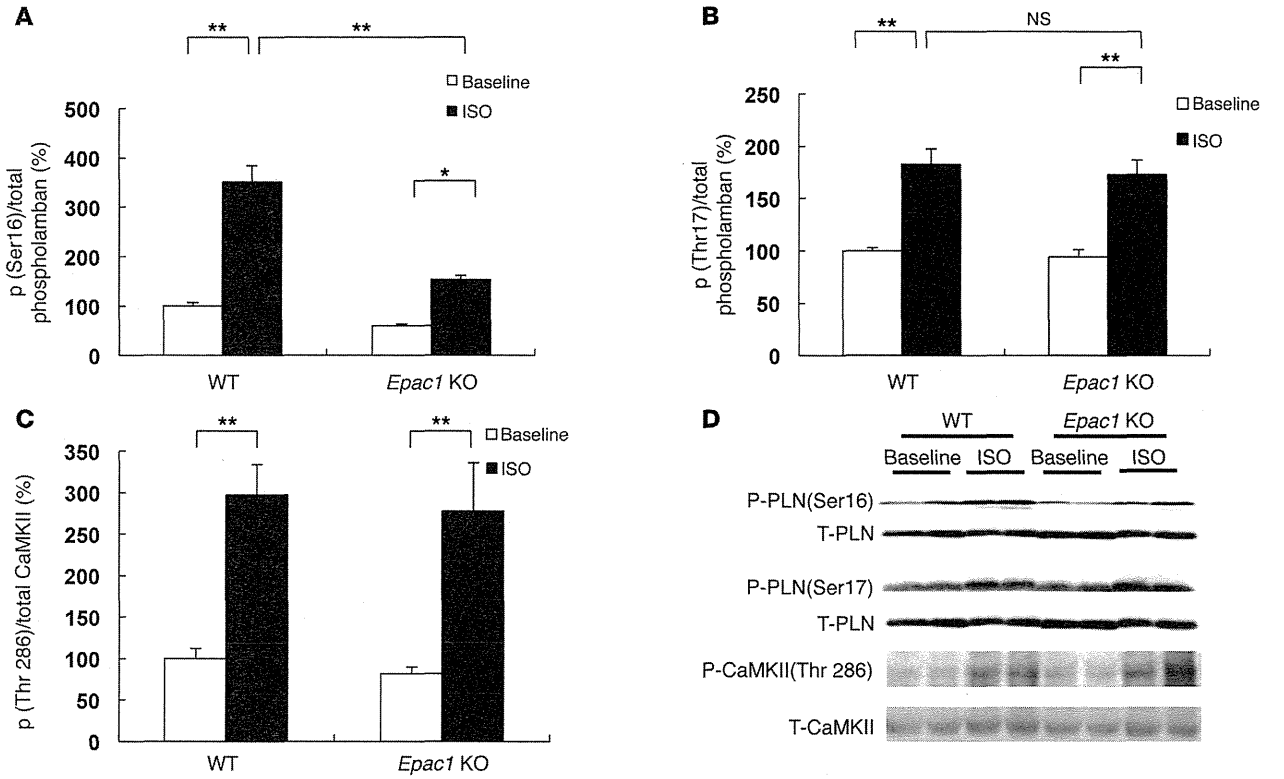

Figure 3

PLN phosphorylation on serine-16 and threonine-17 and CaMKII phosphorylation on threonine-286 in isolated WT or *Epac1* KO heart perfused according to Langendorf method with or without subsequent ISO (0.1 μM) for 5 minutes. (**A**) PLN phosphorylation on serine-16 was significantly increased (*$P < 0.05$, **$P < 0.01$) in response to ISO in WT and *Epac1* KO (WT: from 100% ± 7.0% to 351% ± 32%, $n = 6–8$; *Epac1* KO: from 60 ± 2.6 to 153% ± 9%, $n = 5$), but increase was significantly smaller in *Epac1* KO (153% ± 9%) compared with WT (351% ± 32%, **$P < 0.01$, $n = 5–6$). Ratio of phosphorylated/total protein expression of PLN in WT at baseline was taken as 100%. (**B**) PLN phosphorylation on threonine-17 was similar in WT and *Epac1* KO at baseline and was significantly increased in response to ISO in WT (from 100% ± 2.3% to 183% ± 14%, **$P < 0.01$, $n = 6–8$) and *Epac1* KO (from 94% ± 6.7% to 173% ± 13%, **$P < 0.01$, $n = 6–8$). Magnitudes of the increase were similar (P = NS). Ratio of phosphorylated/total protein expression of PLN in WT at baseline was taken as 100%. (**C**) CaMKII phosphorylation on threonine-286 was similar in WT and *Epac1* KO at baseline and was significantly increased (**$P < 0.01$) in response to ISO in WT (from 100% ± 12% to 297% ± 37%, $n = 5$) and *Epac1* KO (from 82% ± 7.7% to 278% ± 58%, $n = 5$). Magnitudes of increase were similar (P = NS). Ratio of phosphorylated/total protein expression of CaMKII in WT at baseline was taken as 100%. (**D**) Representative immunoblotting results of phosphorylation of PLN on serine-16 (upper) and threonine-17 (middle) and CaMKII on threonine-286 (lower). p-CaMKII, phosphorylated CaMKII; T-CaMKII, total CaMKII.

(7688% ± 497%) relative to that with Bnz-cAMP alone (3324% ± 289%) or with 8-CPT-AM alone (1851% ± 202%) ($P < 0.001$ versus Bnz-cAMP or 8-CPT-AM alone). A similar tendency was observed when 5 μM 8-CPT-AM and 10 μM Bnz-cAMP were used together, suggesting that EPAC-mediated PLN phosphorylation may be independent of PKA-mediated PLN phosphorylation. Taken together, these results indicate that PLN phosphorylation via EPAC is additive to that via PKA, and both EPAC and PKA might be required for maximal PLN activation via phosphorylation on serine-16.

Effects of infection with Ad-PKI-GFP on PLN phosphorylation in neonatal cardiac myocytes transfected with negative or EPAC1 siRNA. In order to confirm the role of EPAC1 in PKA-independent PLN phosphorylation, we generated recombinant adenovirus of mouse protein kinase inhibitor α–GFP (*Pkia*-GFP) infusion gene (Ad-PKI-GFP) and adenovirus of GFP (Ad-GFP) as controls and examined the effects of Ad-PKI-GFP infection on PLN phosphorylation in neonatal rat cardiac myocytes transfected with control or EPAC1 siRNA (Supplemental Figure 9A, Supplemental Figure 10, and ref. 44).

We first confirmed that more than 98% of cells appeared green and that GFP fluorescence was evenly distributed in the cytoplasm of cardiomyocytes infected with Ad-PKI-GFP or Ad-PKI at MOI 100 (Supplemental Figure 10B).

We next performed Western blotting and found that PLN phosphorylation on serine-16 was significantly increased in cells infected with Ad-GFP or Ad-PKI-GFP in addition to control siRNA transfection after ISO treatment (10 μM) for 15 minutes. However, the magnitude of the increase was significantly smaller in cells transfected with Ad-PKI-GFP than with Ad-GFP (Ad-GFP [lane 2] versus Ad-PKI-GFP [lane 4]: 60 ± 2.6 versus 45 ± 3.1-fold, $P < 0.05$, $n = 4$) (Supplemental Figure 10C). In order to examine the role of EPAC1 in PKA-independent PLN phosphorylation on serine-16, we examined the effect of EPAC1 siRNA transfection and found that silencing EPAC1 significantly decreased the ISO-promoted PLN phosphorylation on serine-16 in cells infected with Ad-PKI-GFP (lane 5: 22 ± 0.6-fold, $P < 0.01$, $n = 4$). However, pretreatment with KN-93 (10 μM for 30 minutes), a specific CaMKII inhibitor,

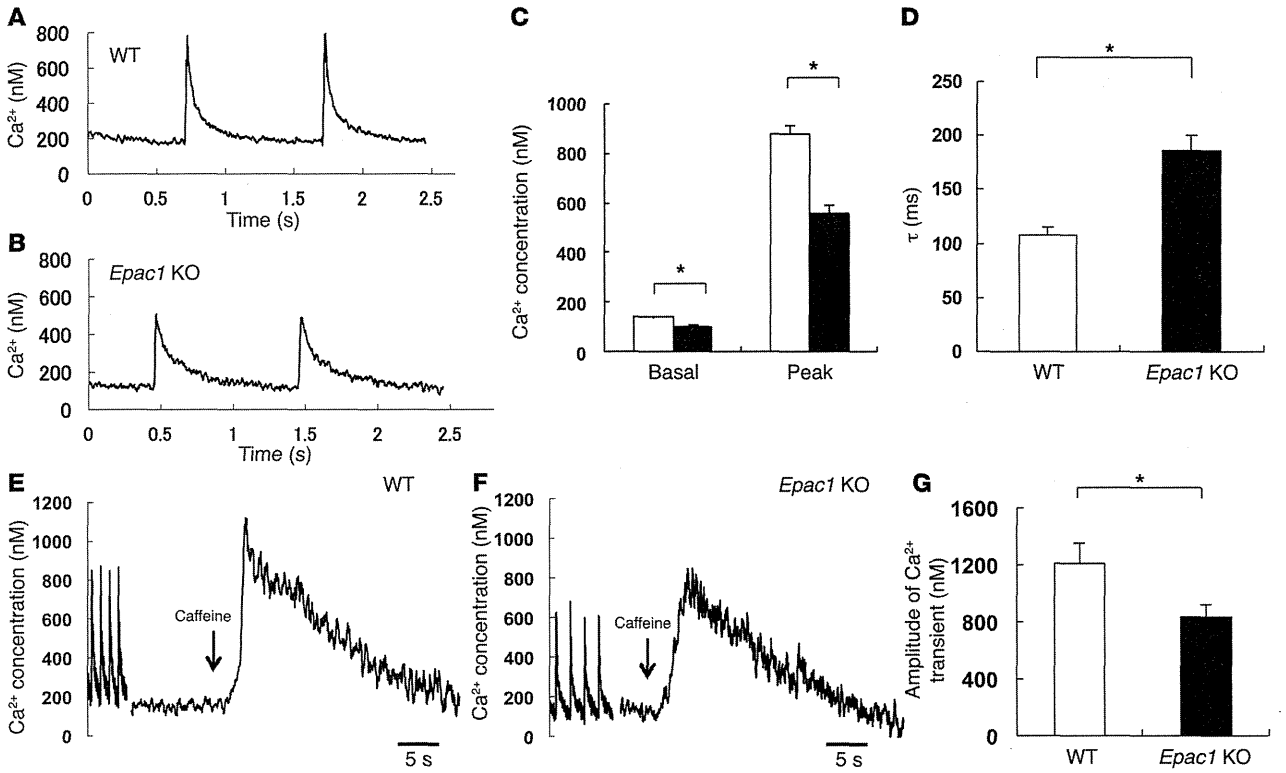

Figure 4

Ca^{2+} transient of adult isolated cardiac myocytes from *Epac1* KO. (**A** and **B**) Typical recordings of Ca^{2+} transients in cardiac myocytes from WT (**A**) and *Epac1* KO (**B**). Note that the basal and peak Ca^{2+} transient amplitude and decay rate are smaller in *Epac1* KO (n = 32 cells from 4 animals each). (**C** and **D**) Ca^{2+} transient parameters of isolated cardiac myocytes from *Epac1* KO and WT. The basal Ca^{2+} concentration (WT versus *Epac1* KO: 139 ± 6.8 versus 99 ± 11.8 nM) and peak Ca^{2+} concentration (WT versus *Epac1* KO: 883 ± 35.3 versus 559 ± 33.2 nM) were significantly lower in *Epac1* KO than in WT (**C**). The decay time constant (τ) was significantly larger in *Epac1* KO than in WT (WT versus *Epac1* KO: 108 ± 6.6 versus 187 ± 13.2 ms) (n = 32 cells, $^*P < 0.05$) (**D**). (**E** and **F**) Typical recordings of Ca^{2+} transients after caffeine (10 mM) treatment of cardiac myocytes from WT (**E**) and *Epac1* KO (**F**). (**G**) Peak Ca^{2+} concentration after caffeine (10 mM) treatment was significantly decreased in *Epac1* KO compared with WT (WT versus *Epac1* KO: 1210 ± 143 versus 835 ± 87.6 nM, n = 7, $^*P < 0.05$).

did not decrease ISO-promoted PLN phosphorylation on serine-16 in cells transfected with control siRNA (lane 6: 37 ± 3.1-fold, P = NS, n = 8) (Supplemental Figure 10C).

We also examined whether PLN phosphorylation on threonine-17 was increased in cells transfected with Ad-GFP or Ad-PKI-GFP in addition to control siRNA after ISO treatment (10 μM) for 15 minutes. However, the magnitudes of the increase were similar in both cases (Ad-GFP [lane 2] versus Ad-PKI-GFP [lane 4]: 59 ± 0.04 versus 56 ± 0.05-fold, P = NS, n = 8) (Supplemental Figure 10D). Transfection of EPAC1 siRNA significantly decreased ISO-promoted PLN phosphorylation on threonine-17 in cells transfected with Ad-PKI-GFP (lane 5: 41 ± 0.04, $P < 0.05$, n = 8) as in the case of serine-16. However, KN-93 pretreatment (10 μM for 30 minutes) abrogated the ISO-promoted PLN phosphorylation on serine-17 in cells transfected with control siRNA (lane 6: 1.4 ± 0.003, $P < 0.01$, n = 8) (Supplemental Figure 10D).

Together with the data in Figure 2D, these data obtained with Ad-PKI-GFP clearly demonstrated that EPAC1 and PKA regulate PLN phosphorylation on serine-16 in an additive and an independent manner. Also, EPAC1 regulates PLN phosphorylation at both serine-16 and threonine-17 in vitro, in addition to PKA and CaMKII.

The increase of PLN phosphorylation on serine-16 with ISO was decreased in Epac1 KO. We next examined the phosphorylation of PLN in total homogenate prepared from WT and *Epac1* KO hearts perfused with the Langendorf method. Hearts were perfused with Krebs solution at constant pressure with or without the treatment of ISO (0.1 μM) for 5 minutes (45), then rapidly frozen in liquid nitrogen for Western blotting (Figure 3).

PLN phosphorylation on serine-16 was significantly decreased in *Epac1* KO compared with that in WT at baseline (WT versus *Epac1* KO: 100% ± 7.0% versus 60% ± 2.5%, $P < 0.05$, n = 5–8). It was significantly increased in response to ISO, but the magnitude of the increase was significantly smaller in *Epac1* KO (WT versus *Epac1* KO: 351% ± 32% versus 153% ± 9%, n = 5–6, $P < 0.01$) (Figure 3A). PLN phosphorylation on threonine-17 was similar in both WT and *Epac1* KO at baseline (100% ± 3.0% versus 94% ± 6.7%, n = 8, P = NS). However, it was significantly increased in both WT and *Epac1* KO in response to ISO ($P < 0.01$), and the magnitudes of the increase were similar (WT versus *Epac1* KO: 183% ± 14% versus 173% ± 13%, n = 6, P = NS) (Figure 3B). CaMKII phosphorylation on threonine-286 was also similar in WT and *Epac1* KO at baseline (WT versus *Epac1*: 100% ± 12% versus 82% ± 7.7%, n = 5, P = NS). It was significantly increased in both WT and *Epac1* KO in response

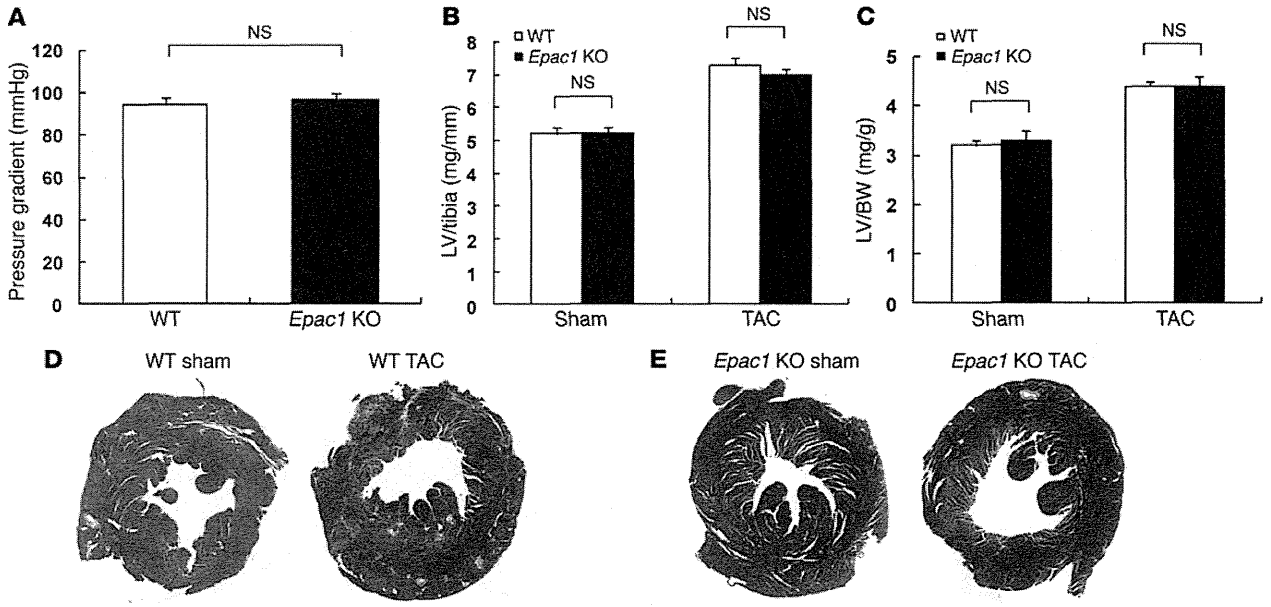

Figure 5

Comparison of cardiac hypertrophy after aortic banding (TAC) in WT and *Epac1* KO. (**A**) Pressure gradients were not different in WT and *Epac1* KO at 3 weeks after TAC (n = 13-16, P = NS). (**B** and **C**) LV weight (mg)/tibial length (mm) ratio (**B**) and LV weight (mg)/body weight (BW, g) ratio (**C**) were determined at 3 weeks. The degree of cardiac hypertrophy was increased at 3 weeks, but was similar in WT and *Epac1* KO (LV/tibial length ratio for WT versus *Epac1* KO: 7.3 ± 0.2 versus 7.0 ± 0.2; LV/BW ratio for WT versus *Epac1* KO: 4.4 ± 0.1 versus 4.4 ± 0.2, n = 18–20, P = NS). (**D** and **E**) Representative gross LV section of Masson-trichrome staining in sham-operated and TAC-operated WT and *Epac1* KO heart. Note that the degree of cardiac hypertrophy was similar, but the fibrotic area after aortic banding was smaller in *Epac1* KO than that in WT.

to ISO (P < 0.01), and the magnitudes of the increase were similar (WT versus *Epac1* KO: 297% ± 37% versus 278% ± 58%, n = 5, P = NS) (Figure 3C). These data indicate that PLN phosphorylation on serine-16, the major site of PKA-mediated phosphorylation, is also regulated by EPAC1. However, EPAC1 does not alter PLN phosphorylation on threonine-17, the major site of CaMKII-mediated phosphorylation, at baseline or in response to ISO.

Silencing EPAC1 in cardiac myocytes attenuates ISO-mediated increases of RyR2 phosphorylations on serine-2808 and serine-2814. PKA and CaMKII-mediated phosphorylation of RyR2 play important roles in modulating cardiac contractility and arrhythmogenesis. It was reported that RyR2 phosphorylation on serine-2808 is mediated by PKA, while RyR2 phosphorylation on serine-2814 is mediated by CaMKII (46). More recently, both sites have been reported to be phosphorylated by PKA and CaMKII, and their phosphorylation is required for adequate RyR2 functional activity (11). We thus examined ISO-induced (10 μM for 3 minutes) phosphorylation on serine-2808 and serine-2814 of RyR2 in neonatal rat cardiac myocytes transfected with control or EPAC1 siRNA because we found that phosphorylated and total RyR2 antibodies did not work well in cardiac homogenate prepared from mouse heart perfused with the Langendorf method (Supplemental Figure 9A and Supplemental Figure 11). RyR2 phosphorylation levels on serine-2808 and serine-2814 were similar in cells transfected with control or EPAC1 siRNA at baseline (serine-2808: control siRNA versus EPAC1 siRNA: 100% ± 1.9% versus 130% ± 4.9%, n = 4, P = NS; serine-2814: control siRNA versus EPAC1 siRNA: 100% ± 16% versus 116% ± 16%, n = 4–6, P = NS). They were significantly increased in response to ISO, but the magnitudes of the increase on both serine-2808 (Supplemental Figure 11B) and serine-2814 (Supplemental Figure 11C) were significantly smaller in cells transfected with EPAC1 siRNA than those in cells transfected with control siRNA (serine-2808: control siRNA versus EPAC1 siRNA 268% ± 8.3% versus 199% ± 13%; P < 0.01, n = 6; serine-2814: control siRNA versus EPAC1 siRNA 220% ± 13% versus 170% ± 2.3%, P < 0.05, n = 4–6). These data indicate that EPAC1 regulates RyR2 phosphorylation on serine-2808 and serine-2814 in addition to PKA and CaMKII.

Intracellular Ca^{2+} concentration is decreased in Epac1 KO myocytes. Cardiac contraction and relaxation are influenced by the intracellular increase in Ca^{2+} during systole and its decrease during diastole. Sarcoplasmic reticulum Ca^{2+} uptake is regulated via PLN phosphorylation. PLN phosphorylation has recently been concluded to play a prominent role in the regulation of myocardial contraction as well as relaxation based on findings in *Pln* knockout mice (12).

We thus examined the intracellular Ca^{2+} concentration in isolated cardiac myocytes of *Epac1* KO (Figure 4, A and B). The basal and peak Ca^{2+} concentrations were significantly decreased in *Epac1* KO compared with WT (basal Ca^{2+} in WT versus *Epac1* KO 139 ± 6.8 versus 99 ± 11.8 nM, n = 32, P < 0.01; peak Ca^{2+} in WT versus *Epac1* KO: 883 ± 35.3 versus 559 ± 33.2 nM, n = 32, P < 0.01) (Figure 4C). The decay time constant (τ) was significantly larger in *Epac1* KO than that in WT controls (WT versus *Epac1* KO: 108 ± 6.6 versus 187 ± 13.2 ms, n = 32, P < 0.01) (Figure 4D). We also examined the cytoplasmic Ca^{2+} concentration after addition of caffeine (10 mM) as a measure of Ca^{2+} content in SR in isolated cardiac myocytes of WT and *Epac1* KO (Figure 4, E–G). The amplitude of the caffeine-induced increase in cytoplasmic Ca^{2+} concentration was significant in WT compared with *Epac1*

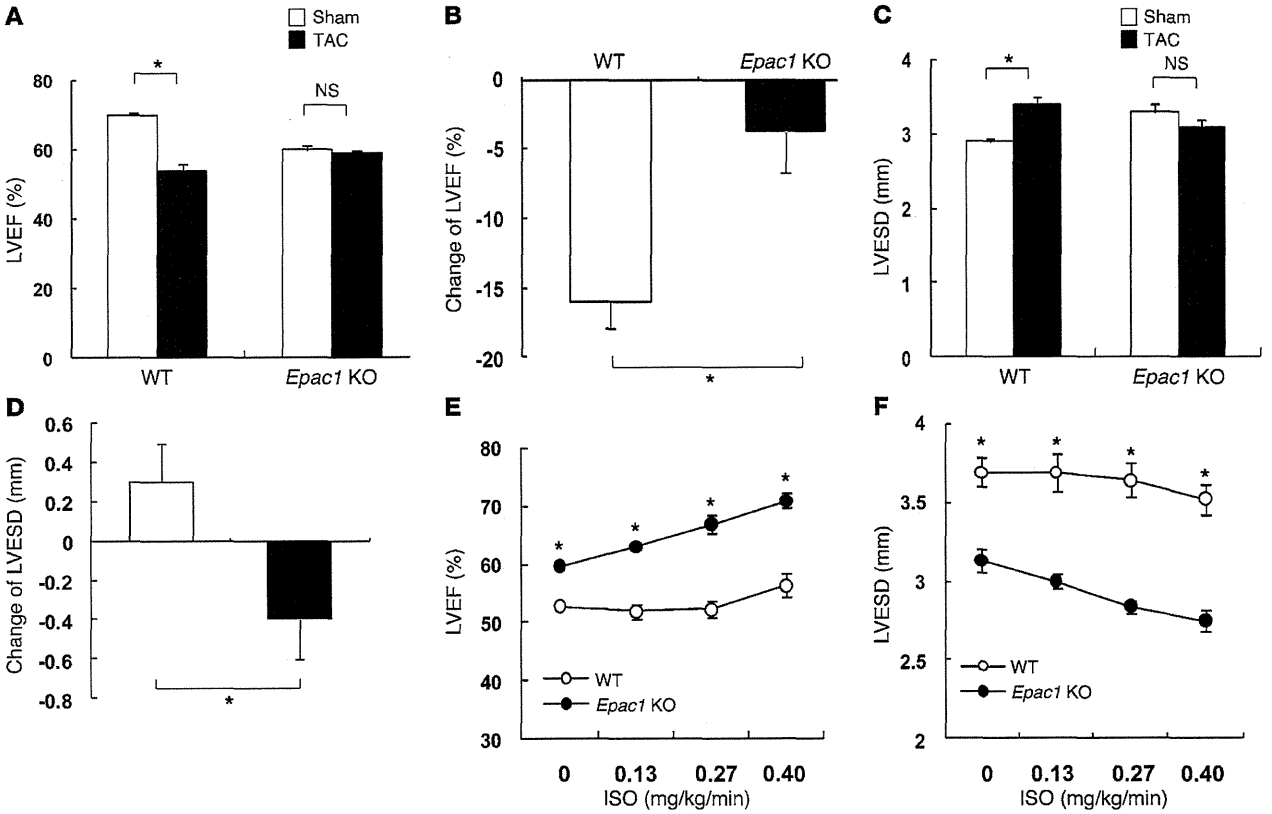

Figure 6

Changes in LV function at 3 weeks after aortic banding (TAC) in WT and *Epac1* KO. Echocardiographic measurements of LV function were performed at 3 weeks after TAC of WT and *Epac1* KO and in sham-operated controls. (**A** and **B**) LVEF was significantly decreased in WT (*$P < 0.01$), but not in *Epac1* KO (P = NS) at 3 weeks (WT versus *Epac1* KO: from 70% ± 0.8% to 54% ± 2.0% versus from 60% ± 1.1% to 59% ± 0.7%, n = 17–30) (**A**). The data were compared with those from sham-operated controls at 3 weeks in each mouse. Change of LVEF from sham-operated controls at 3 weeks after TAC was significantly greater in WT than that in *Epac1* KO (**B**) (n = 17–31, *$P < 0.01$). (**C** and **D**) LVESD was significantly increased in WT, but not in *Epac1* KO at 3 weeks after TAC (**C**). The data were compared with those from sham-operated controls at 3 weeks. Change of LVESD from sham-operated controls at 3 weeks after banding was greater in WT than that in *Epac1* KO (n = 17–31, *$P < 0.01$) (**D**). The decrease of LVESD in response to intravenous acute ISO infusion (0, 0.13, 0.27, 0.40 mg/kg/min for 5 minutes) was depressed in WT, but not in *Epac1* KO (n = 4–5, *$P < 0.01$). (**E** and **F**) The increase of LVEF (**E**) and the decrease of LVESD (**F**) in response to intravenous acute ISO infusion (0, 0.13, 0.27, 0.40 mg/kg/min for 5 minutes) were depressed in WT, but not in *Epac1* KO (n = 4–5, *$P < 0.01$) (**E**).

KO (WT versus *Epac1* KO: 1210 ± 143 versus 835 ± 87.6 nM, n = 7, $P < 0.05$), indicating that the Ca^{2+} content in SR was decreased in *Epac1* KO compared with WT.

Activities of L-type Ca^{2+} channel and NCX channel in Epac1 KO are similar to those in WT. We measured the L-type Ca^{2+} channel current (I_{CaL}) and Na^{+}-Ca^{2+} exchange current (I_{NCX}) using the cell patch-clamp technique in isolated cardiac myocytes of *Epac1* KO and confirmed that the density and current-voltage relationships of I_{CaL} (Supplemental Figure 12) and I_{NCX} (Supplemental Figure 13) were not different. We also examined the response of I_{CaL}, a PKA-dependent target, in response to ISO (10^{-7} M) and confirmed that it was not different between WT and *Epac1* KO (Supplemental Figure 12B and ref. 6).

Disruption of EPAC1 does not affect development of cardiac hypertrophy, but prevents heart failure in pressure overload stress. In order to examine the role of EPAC1 in the development of heart failure, we performed aortic banding in *Epac1* KO and WT for 3 weeks. The pressure gradients were similar in WT and *Epac1* KO at 3 weeks after banding (Figure 5A). At baseline, there was no difference between WT and *Epac1* KO in the LV weight (mg)/tibial length (mm) (LV/tibial length ratio in WT versus *Epac1* KO: 5.2 ± 0.2 versus 5.2 ± 0.2 mg/mm, n = 18–20, P = NS). The degree of cardiac hypertrophy was increased at 3 weeks, but remained similar in *Epac1* KO and WT (LV/tibial length ratio in WT versus *Epac1* KO: 7.3 ± 0.2 versus 7.0 ± 0.2, n = 18–20, P = NS) (Figure 5, B, D, and E). The change of LV/body weight ratio, another index of cardiac hypertrophy, confirmed the finding based on LV/tibial length ratio (WT versus *Epac1* KO: from 3.2 ± 0.1 to 4.4 ± 0.1 versus from 3.3 ± 0.2 to 4.4 ± 0.2 mg/g, n = 18–20, P = NS) (Figure 5C).

At 3 weeks after banding, however, cardiac function (LVEF) was significantly decreased in WT ($P < 0.01$), while it remained unchanged in *Epac1* KO (WT versus *Epac1* KO: from 70% ± 0.8% to 54% ± 2.0% versus from 60% ± 1.1% to 60% ± 0.7%, n = 17–30) (Figure 6, A and B). LVESD was increased significantly in WT at 3 weeks after banding ($P < 0.01$), while it remained unchanged in *Epac1* KO (WT versus *Epac1* KO: from 2.9 ± 0.04 to 3.3 ± 0.1 versus from 3.4 ± 0.1 to 3.1 ± 0.1 mm, n = 17–31) (Figure 6, C and D). Hemodynamic measurements demonstrated that Max dP/dt was significantly decreased in WT, but not in *Epac1*